

Bottomonium-like tetraquarks in a chiral quark model

Gang Yang,^{1,*} Jialun Ping,^{2,†} and Jorge Segovia^{3,‡}

¹*Department of Physics, Zhejiang Normal University, Jinhua 321004, China*

²*Department of Physics and Jiangsu Key Laboratory for Numerical Simulation of Large Scale Complex Systems, Nanjing Normal University, Nanjing 210023, P. R. China*

³*Departamento de Sistemas Físicos, Químicos y Naturales, Universidad Pablo de Olavide, E-41013 Sevilla, Spain*

(Dated: April 20, 2022)

The low-lying bottomonium-like tetraquarks $b\bar{b}q\bar{q}$ ($q = u, d, s$) with spin-parity $J^P = 0^+, 1^+$ and 2^+ , and isospin $I = 0, 1$ or $\frac{1}{2}$, are systematically investigated within the theoretical framework of real- and complex-scaling range of a chiral quark model, which has already been successfully applied in analysis of several multi-quark systems. A complete four-body S -wave function, which includes meson-meson, diquark-antidiquark and K -type arrangements of quarks, along with all possible color configurations are considered. In the $b\bar{b}q\bar{q}$ ($q = u, d$) tetraquark system, we found resonance states of $B^{(*)}\bar{B}^{(*)}$, $\Upsilon\omega$, $\Upsilon\rho$ and $\eta_b\rho$ nature with all possible $I(J^P)$ quantum numbers. Their masses are generally located in the energy range 11.0 – 11.3 GeV and their widths are less than 10 MeV. In addition, extremely narrow resonances, with two-meson strong decay widths less than 1.5 MeV, are obtained in both $b\bar{b}u\bar{s}$ and $b\bar{b}s\bar{s}$ tetraquark systems. Particularly, four radial excitations of ΥK^* and $\eta_b K^*$ are found at ~ 11.1 GeV in $J^P = 0^+, 1^+$ and 2^+ channels of $b\bar{b}u\bar{s}$ system. One $\Upsilon(1S)\phi(2S)$ resonance state is obtained at 11.28 GeV in the $J^P = 1^+$ sector.

I. INTRODUCTION

During the past two decades several exotic structures have been reported experimentally, and this fact undoubtedly opens crucial access in exploring the quantum field theory of the strong interaction, *i.e.* Quantum Chromodynamics (QCD), and its related perturbative and non-perturbative theoretical formulations; in particular, QCD-inspired phenomenological quark models and their extensions.

Focusing on the most recent discoveries, on one hand, the first hidden-charm pentaquark $P_c^+(4380)$ was announced by the LHCb collaboration in 2015 [1]; later on, many more candidates of exotic hadrons with 5-quark content were reported, *e.g.*, the $P_c^+(4312)$, $P_c^+(4337)$, $P_c^+(4440)$ and $P_c^+(4457)$ [2, 3], and the hidden-charm pentaquark with strangeness $P_{cs}^0(4459)$ [4]. On the other hand, substantial data on tetraquark candidates have been accumulated in the last two years by worldwide high-energy experiments such as the LHCb, BES III and Belle II. Particularly, there are several open- and hidden-charm structures newly reported, such as the charm-strange tetraquarks $X_{0,1}(2900)$ [5, 6], the doubly charmed tetraquark T_{cc}^+ [7, 8], the charged hidden-charm tetraquarks with strangeness $Z_{cs}(3985)$ [9], $Z_{cs}(4000)$, $Z_{cs}(4220)$, $X(4630)$ and $X(4685)$ [10], and the fully charmed tetraquark $X(6900)$ [11].

The experimental progress within hidden-bottom sector can be dated back to 2011, when two charged exotic candidates $Z_b(10610)$ and $Z_b(10650)$ were reported by the Belle collaboration [12], and confirmed in later

studies [13, 14]. A wide range of phenomenological approaches have been employed in investigating their properties. Generally, a $B^{(*)}\bar{B}^*$ molecule interpretation for these Z_b hadrons is favored by effective field theory [15, 16], phenomenology models [17–19] and heavy quark symmetry [20]. However, either virtual state or cusp effects may be not discarded [21–24]. Meanwhile, a $b\bar{b}u\bar{d}$ tetraquark has been very recently studied in lattice-regularized QCD and no significant attraction, or repulsion, is found [25]; in contrast, several attraction features of $B_s^{(*)}B_s^{(*)}$ systems have been suggested by effective field theory investigation [26]. A way of distinguishing among the mentioned structural solutions is studying the decay properties of $Z_b(10610)$ and $Z_b(10650)$ which have been analyzed in quark model approaches [27, 28].

The exciting advances in the exploration of exotic hadrons with heavy quark content have triggered many theoretical studies using a wide variety of approaches. Comprehensive reviews of the status of the field have been published over the years [29–36]. Given the fact that several hidden-charm tetraquarks with strangeness have been just experimentally reported along the last year, and they have been investigated by us within a chiral quark model formalism [37], a natural extension to the bottomonium-like tetraquark $b\bar{b}q\bar{q}$ ($q = u, d, s$) investigation is proposed herein.

A QCD-based chiral quark model is employed, and this formalism has already been successfully applied in the study of a wide variety of multi-quark systems, *e.g.* hidden- and double-charm pentaquarks [38, 39], hidden-bottom pentaquarks [40], doubly and fully heavy tetraquarks [41–43], and one-heavy-quark tetraquarks with strangeness [44]. The formulation of our chiral quark model in either real- and complex-scaling method has been discussed extensively in Ref. [34], which serves also as a nice review of our latest results for multi-quark

* yanggang@zjnu.edu.cn

† jlping@njnu.edu.cn

‡ jsegovia@upo.es

systems. The complex-scaling method (CSM) allows us to distinguish bound, resonance and continuum states directly, and thus perform a complete analysis of the scattering singularities within the same formalism. Furthermore, the meson-meson, diquark-antidiquark and K-type configurations, plus their couplings, shall be considered for the $b\bar{b}q\bar{q}$ tetraquark system with all possible color configurations.

The manuscript is arranged as follows. In Sec. II the theoretical framework is presented; we briefly discuss the complex-range method applied to a chiral quark model and the $b\bar{b}q\bar{q}$ ($q = u, d, s$) tetraquark wave-functions. Section III is devoted to the analysis of the obtained low-lying bottomonium-like tetraquark states with $J^P = 0^+, 1^+$ and 2^+ , and isospin $I = 0, 1$ or $\frac{1}{2}$. And, finally, a summary is presented in Sec. IV.

II. THEORETICAL FRAMEWORK

A throughout review of the theoretical formalism used herein has been recently published in Ref. [34]. We shall, however, focused on the most relevant features of the chiral quark model and the numerical method concerning the hidden-bottom tetraquarks $b\bar{b}q\bar{q}$ ($q = u, d, s$).

Within the so-called complex-range studies, the relative coordinate of a two-body interaction is rotated in the complex plane by an angle θ , *i.e.*, $\vec{r}_{ij} \rightarrow \vec{r}_{ij}e^{i\theta}$. Therefore, the general form of the four-body Hamiltonian reads:

$$H(\theta) = \sum_{i=1}^4 \left(m_i + \frac{\vec{p}_i^2}{2m_i} \right) - T_{\text{CM}} + \sum_{j>i=1}^4 V(\vec{r}_{ij}e^{i\theta}), \quad (1)$$

where m_i and \vec{p}_i are, respectively, the mass and momentum of a quark; and T_{CM} is the center-of-mass kinetic energy. According to the so-called ABC theorem [45, 46], the complex scaled Schrödinger equation:

$$[H(\theta) - E(\theta)] \Psi_{JM}(\theta) = 0 \quad (2)$$

has (complex) eigenvalues which can be classified into three types, namely bound, resonance and scattering states. In particular, bound-states and resonances are independent of the rotated angle θ , with the first ones always fixed on the real-axis (there is no imaginary part of the eigenvalue), and the second ones located above the continuum threshold with a total decay width $\Gamma = -2\text{Im}(E)$.

The dynamics of the $b\bar{b}q\bar{q}$ tetraquark system is driven by a two-body potential

$$V(\vec{r}_{ij}) = V_\chi(\vec{r}_{ij}) + V_{\text{CON}}(\vec{r}_{ij}) + V_{\text{OGE}}(\vec{r}_{ij}), \quad (3)$$

which takes into account the most relevant features of QCD at its low energy regime: dynamical chiral symmetry breaking, confinement and the perturbative one-gluon exchange interaction. Herein, the low-lying S -wave positive parity $b\bar{b}q\bar{q}$ tetraquark states shall be investigated,

and thus the central and spin-spin terms of the potential are the only ones needed.

One consequence of the dynamical breaking of chiral symmetry is that Goldstone boson exchange interactions appear between constituent light quarks u, d and s . Therefore, the chiral interaction can be written as [47]:

$$V_\chi(\vec{r}_{ij}) = V_\pi(\vec{r}_{ij}) + V_\sigma(\vec{r}_{ij}) + V_K(\vec{r}_{ij}) + V_\eta(\vec{r}_{ij}), \quad (4)$$

given by

$$V_\pi(\vec{r}_{ij}) = \frac{g_{ch}^2}{4\pi} \frac{m_\pi^2}{12m_i m_j} \frac{\Lambda_\pi^2}{\Lambda_\pi^2 - m_\pi^2} m_\pi \left[Y(m_\pi r_{ij}) - \frac{\Lambda_\pi^3}{m_\pi^3} Y(\Lambda_\pi r_{ij}) \right] (\vec{\sigma}_i \cdot \vec{\sigma}_j) \sum_{a=1}^3 (\lambda_i^a \cdot \lambda_j^a), \quad (5)$$

$$V_\sigma(\vec{r}_{ij}) = -\frac{g_{ch}^2}{4\pi} \frac{\Lambda_\sigma^2}{\Lambda_\sigma^2 - m_\sigma^2} m_\sigma \left[Y(m_\sigma r_{ij}) - \frac{\Lambda_\sigma}{m_\sigma} Y(\Lambda_\sigma r_{ij}) \right], \quad (6)$$

$$V_K(\vec{r}_{ij}) = \frac{g_{ch}^2}{4\pi} \frac{m_K^2}{12m_i m_j} \frac{\Lambda_K^2}{\Lambda_K^2 - m_K^2} m_K \left[Y(m_K r_{ij}) - \frac{\Lambda_K^3}{m_K^3} Y(\Lambda_K r_{ij}) \right] (\vec{\sigma}_i \cdot \vec{\sigma}_j) \sum_{a=4}^7 (\lambda_i^a \cdot \lambda_j^a), \quad (7)$$

$$V_\eta(\vec{r}_{ij}) = \frac{g_{ch}^2}{4\pi} \frac{m_\eta^2}{12m_i m_j} \frac{\Lambda_\eta^2}{\Lambda_\eta^2 - m_\eta^2} m_\eta \left[Y(m_\eta r_{ij}) - \frac{\Lambda_\eta^3}{m_\eta^3} Y(\Lambda_\eta r_{ij}) \right] (\vec{\sigma}_i \cdot \vec{\sigma}_j) \left[\cos \theta_p (\lambda_i^8 \cdot \lambda_j^8) - \sin \theta_p \right], \quad (8)$$

where $Y(x) = e^{-x}/x$ is the standard Yukawa function. The physical η meson, instead of the octet one, is considered by introducing the angle θ_p . The λ^a are the SU(3) flavor Gell-Mann matrices. Taken from their experimental values, m_π , m_K and m_η are the masses of the SU(3) Goldstone bosons.

The value of m_σ is given by the partially conserved axial current relation $m_\sigma^2 \simeq m_\pi^2 + 4m_{u,d}^2$ [48]. Note, however, that better determinations of the mass of the σ -meson have been reported since then [49, 50] – see also the recent review [51]; one should simply consider the value used here as a model parameter. Finally, the chiral coupling constant, g_{ch} , is determined from the πNN coupling constant through

$$\frac{g_{ch}^2}{4\pi} = \frac{9}{25} \frac{g_{\pi NN}^2}{4\pi} \frac{m_{u,d}^2}{m_N^2}, \quad (9)$$

which assumes that flavor SU(3) is an exact symmetry only broken by the different mass of the strange quark.

Color confinement should be encoded in the non-Abelian character of QCD. An attractive linearly rising potential proportional to the distance between infinite-heavy quarks is the consequence of multi-gluon exchanges as demonstrated by lattice-regularized QCD [52]. However, the spontaneous creation of light-quark pairs from the QCD vacuum may give rise at the same scale to a breakup of the created color flux-tube [52]. These two observations can be phenomenologically described by [53]:

$$V_{\text{CON}}(\vec{r}_{ij}) = [-a_c(1 - e^{-\mu_c r_{ij}}) + \Delta] (\lambda_i^c \cdot \lambda_j^c), \quad (10)$$

where a_c , μ_c and Δ are model parameters, and the SU(3) color Gell-Mann matrices are denoted as λ^c . One can see in Eq. (10) that the potential is linear at short interquark distances with an effective confinement strength $\sigma = -a_c \mu_c (\lambda_i^c \cdot \lambda_j^c)$, while it becomes constant at large distances, $V_{\text{thr.}} = (\Delta - a_c)(\lambda_i^c \cdot \lambda_j^c)$.

Beyond the chiral symmetry breaking scale one expects the dynamics to be governed by QCD perturbative effects. In particular, the one-gluon exchange potential, which includes the so-called coulomb and color-magnetism interactions, is the leading order contribution:

$$V_{\text{OGE}}(\vec{r}_{ij}) = \frac{1}{4} \alpha_s (\lambda_i^c \cdot \lambda_j^c) \left[\frac{1}{r_{ij}} - \frac{1}{6m_i m_j} (\vec{\sigma}_i \cdot \vec{\sigma}_j) \frac{e^{-r_{ij}/r_0(\mu_{ij})}}{r_{ij} r_0^2(\mu_{ij})} \right], \quad (11)$$

where $r_0(\mu_{ij}) = \hat{r}_0/\mu_{ij}$ is a regulator which depends on the reduced mass of the $q\bar{q}$ pair, the Pauli matrices are denoted by $\vec{\sigma}$, and the contact term has been regularized as

$$\delta(\vec{r}_{ij}) \sim \frac{1}{4\pi r_0^2(\mu_{ij})} \frac{e^{-r_{ij}/r_0(\mu_{ij})}}{r_{ij}}. \quad (12)$$

An effective scale-dependent strong coupling constant, $\alpha_s(\mu_{ij})$, provides a consistent description of mesons and baryons from light to heavy quark sectors. We use the frozen coupling constant of, for instance, Ref. [54]

$$\alpha_s(\mu_{ij}) = \frac{\alpha_0}{\ln\left(\frac{\mu_{ij}^2 + \mu_0^2}{\Lambda_0^2}\right)}, \quad (13)$$

in which α_0 , μ_0 and Λ_0 are parameters of the model.

The model parameters are listed in Table I. They have been fixed in advance reproducing hadron [55–60], hadron-hadron [61–66] and multi-quark [38, 40, 44, 67–69] phenomenology. Additionally, for later concern, Table II lists theoretical and experimental (if available) masses of $1S$, $2S$ and $3S$ states of $q\bar{q}$, $b\bar{q}$ ($q = u, d, s$) and $b\bar{b}$ mesons.

Figure 1 shows seven kinds of configurations for the $b\bar{b}q\bar{q}$ tetraquark system. In particular, panels 1(a) and (b) are the meson-meson structures, panel 1(c) is the diquark-antidiquark one, and the other K-type configurations are from panels (d) to (g). All of them, and their

TABLE I. Model parameters.

Quark masses	m_q ($q = u, d$) (MeV)	313
	m_s (MeV)	555
	m_b (MeV)	5100
Goldstone bosons	$\Lambda_\pi = \Lambda_\sigma$ (fm $^{-1}$)	4.20
	$\Lambda_\eta = \Lambda_K$ (fm $^{-1}$)	5.20
	$g_{ch}^2/(4\pi)$	0.54
	θ_P ($^\circ$)	-15
Confinement	a_c (MeV)	430
	μ_c (fm $^{-1}$)	0.70
	Δ (MeV)	181.10
OGE	α_0	2.118
	Λ_0 (fm $^{-1}$)	0.113
	μ_0 (MeV)	36.976
	\hat{r}_0 (MeV fm)	28.170

couplings, are considered in our investigation. However, for the purpose of solving a manageable 4-body problem, the K-type configurations are sometimes restricted, following a similar criteria as our investigation on the hidden-charm tetraquarks with strangeness [37]. Furthermore, it is important to note herein that just one configuration would be enough for the calculation, if all radial and orbital excited states were taken into account; however, this is obviously much less efficient and thus an economic way is to combine the different configurations in the ground state to perform the calculation.

The multi-quark system's wave function at the quark level is an internal product of color, spin, flavor and space terms. Concerning the color degree-of-freedom, the colorless wave function of a 4-quark system in meson-meson configuration, as illustrated in Fig. 1(a) and (b), can be obtained by either two coupled color-singlet clusters, $1 \otimes 1$:

$$\chi_1^c = \frac{1}{3} (\bar{r}r + \bar{g}g + \bar{b}b) \times (\bar{r}r + \bar{g}g + \bar{b}b), \quad (14)$$

or two coupled color-octet clusters, $8 \otimes 8$:

$$\begin{aligned} \chi_2^c = & \frac{\sqrt{2}}{12} (3\bar{b}r\bar{r}b + 3\bar{g}r\bar{r}g + 3\bar{b}g\bar{g}b + 3\bar{g}b\bar{b}g + 3\bar{r}g\bar{g}r \\ & + 3\bar{r}b\bar{b}r + 2\bar{r}r\bar{r}r + 2\bar{g}g\bar{g}g + 2\bar{b}b\bar{b}b - \bar{r}r\bar{g}g \\ & - \bar{g}g\bar{r}r - \bar{b}b\bar{g}g - \bar{b}b\bar{r}r - \bar{g}g\bar{b}b - \bar{r}r\bar{b}b). \end{aligned} \quad (15)$$

The first color state is the so-called color-singlet channel and the second one is named as the hidden-color case.

The color wave functions associated to the diquark-antidiquark structure shown in Fig. 1(c) are the coupled

TABLE II. Theoretical and experimental (if available) masses of $nL = 1S, 2S$ and $3S$ states of $q\bar{q}, q\bar{b}$ ($q = u, d, s$) and $b\bar{b}$ mesons.

Meson	nL	$M_{\text{The.}}$ (MeV)	$M_{\text{Exp.}}$ (MeV)	Meson	nL	$M_{\text{The.}}$ (MeV)	$M_{\text{Exp.}}$ (MeV)
π	1S	149	140	η	1S	689	548
	2S	1291	1300		2S	1443	1295
	3S	1749	1800		3S	1888	-
ρ	1S	772	770	ω	1S	696	782
	2S	1479	1450		2S	1449	1420
	3S	1940	-		3S	1897	1650
K	1S	481	494	K^*	1S	907	892
	2S	1468	1460		2S	1621	1630
	3S	1898	1830		3S	1998	-
η'	1S	828	958	ϕ	1S	1011	1020
	2S	1639	1760		2S	1720	1680
	3S	2057	-		3S	2097	2170
B	1S	5278	5280	B^*	1S	5319	5325
	2S	5984	-		2S	6005	-
	3S	6373	-		3S	6383	-
B_s	1S	5355	5367	B_s^*	1S	5400	5415
	2S	6017	-		2S	6042	-
	3S	6412	-		3S	6432	-
η_b	1S	9454	9300	Υ	1S	9505	9460
	2S	9985	-		2S	10013	10023
	3S	10327	-		3S	10345	10355

color triplet-antitriplet clusters, $3 \otimes \bar{3}$:

$$\chi_3^c = \frac{\sqrt{3}}{6} (\bar{r}r\bar{g}g - \bar{g}r\bar{r}g + \bar{g}g\bar{r}r - \bar{r}g\bar{g}r + \bar{r}r\bar{b}b - \bar{b}r\bar{r}b + \bar{b}b\bar{r}r - \bar{r}b\bar{b}r + \bar{g}g\bar{b}b - \bar{b}g\bar{g}b + \bar{b}b\bar{g}g - \bar{g}b\bar{b}g), \quad (16)$$

and the coupled color sextet-antisextet clusters, $6 \otimes \bar{6}$:

$$\chi_4^c = \frac{\sqrt{6}}{12} (2\bar{r}r\bar{r}r + 2\bar{g}g\bar{g}g + 2\bar{b}b\bar{b}b + \bar{r}r\bar{g}g + \bar{g}r\bar{r}g + \bar{g}g\bar{r}r + \bar{r}g\bar{g}r + \bar{r}r\bar{b}b + \bar{b}r\bar{r}b + \bar{b}b\bar{r}r + \bar{r}b\bar{b}r + \bar{g}g\bar{b}b + \bar{b}g\bar{g}b + \bar{b}b\bar{g}g + \bar{g}b\bar{b}g). \quad (17)$$

Meanwhile, the colorless wave functions of the K-type structures shown in Fig. 1(d) to (g) are

$$\chi_5^c = \frac{1}{6\sqrt{2}} (\bar{r}r\bar{r}r + \bar{g}g\bar{g}g - 2\bar{b}b\bar{b}b) + \frac{1}{2\sqrt{2}} (\bar{r}b\bar{b}r + \bar{r}g\bar{g}r + \bar{g}b\bar{b}g + \bar{g}r\bar{r}g + \bar{b}g\bar{g}b + \bar{b}r\bar{r}b) - \frac{1}{3\sqrt{2}} (\bar{g}g\bar{r}r + \bar{r}r\bar{g}g) + \frac{1}{6\sqrt{2}} (\bar{b}b\bar{r}r + \bar{b}b\bar{g}g + \bar{r}r\bar{b}b + \bar{g}g\bar{b}b), \quad (18)$$

$$\chi_6^c = \chi_1^c, \quad (19)$$

$$\chi_7^c = \chi_1^c, \quad (20)$$

$$\chi_8^c = \frac{1}{4} (1 - \frac{1}{\sqrt{6}}) \bar{r}r\bar{g}g - \frac{1}{4} (1 + \frac{1}{\sqrt{6}}) \bar{g}g\bar{g}g - \frac{1}{4\sqrt{3}} \bar{r}g\bar{g}r + \frac{1}{2\sqrt{2}} (\bar{r}b\bar{b}r + \bar{g}b\bar{b}g + \bar{b}g\bar{g}b + \bar{g}r\bar{r}g + \bar{b}r\bar{r}b) + \frac{1}{2\sqrt{6}} (\bar{r}r\bar{b}b - \bar{g}g\bar{b}b + \bar{b}b\bar{g}g + \bar{g}g\bar{r}r - \bar{b}b\bar{r}r), \quad (21)$$

$$\chi_9^c = \frac{1}{2\sqrt{6}} (\bar{r}b\bar{b}r + \bar{r}r\bar{b}b + \bar{g}b\bar{b}g + \bar{g}g\bar{b}b + \bar{r}g\bar{g}r + \bar{r}r\bar{g}g + \bar{b}b\bar{g}g + \bar{b}g\bar{g}b + \bar{g}g\bar{r}r + \bar{g}r\bar{r}g + \bar{b}b\bar{r}r + \bar{b}r\bar{r}b) + \frac{1}{\sqrt{6}} (\bar{r}r\bar{r}r + \bar{g}g\bar{g}g + \bar{b}b\bar{b}b), \quad (22)$$

$$\chi_{10}^c = \frac{1}{2\sqrt{3}} (\bar{r}b\bar{b}r - \bar{r}r\bar{b}b + \bar{g}b\bar{b}g - \bar{g}g\bar{b}b + \bar{r}g\bar{g}r - \bar{r}r\bar{g}g - \bar{b}b\bar{g}g + \bar{b}g\bar{g}b - \bar{g}g\bar{r}r + \bar{g}r\bar{r}g - \bar{b}b\bar{r}r + \bar{b}r\bar{r}b), \quad (23)$$

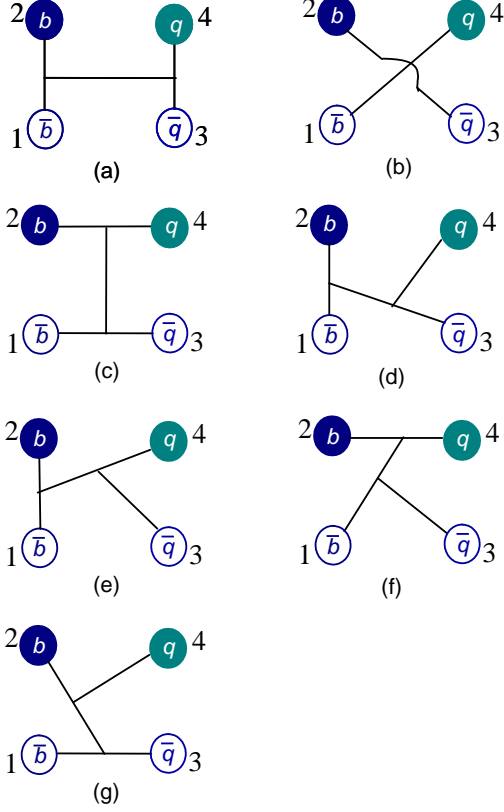


FIG. 1. Seven types of configurations in $b\bar{b}q\bar{q}$ ($q = u, d, s$) tetraquarks. Panels (a) and (b) represent meson-meson structures, panel (c) is diquark-antidiquark one and the other K-type structures are shown in panels (d) to (g).

$$\chi_{11}^c = \chi_9^c, \quad (24)$$

$$\chi_{12}^c = -\chi_{10}^c. \quad (25)$$

According to the nature of $SU(3)$ flavor, $b\bar{b}q\bar{q}$ ($q = u, d, s$) tetraquark systems could be categorized into three parts, *i.e.* $b\bar{b}q\bar{q}$, $b\bar{b}q\bar{s}$ and $b\bar{b}s\bar{s}$ ($q = u, d$). The flavor wave function is then denoted as χ_{I, M_I}^{fi} , where the superscript f just indicates *flavor* part of the wave function and $i = 1, 2$ and 3 will refer to $b\bar{b}q\bar{q}$, $b\bar{b}q\bar{s}$ ($q = u, d$) and $b\bar{b}s\bar{s}$ systems, respectively. We have isoscalar, $I = 0$, and isovector, $I = 1$, sectors in the $b\bar{b}q\bar{q}$ system, their flavor wave functions read as

$$\chi_{0,0}^{fi} = -\frac{1}{\sqrt{2}}(\bar{b}b\bar{u}u + \bar{b}b\bar{d}d), \quad (26)$$

$$\chi_{1,0}^{fi} = -\frac{1}{\sqrt{2}}(\bar{b}b\bar{u}u - \bar{b}b\bar{d}d). \quad (27)$$

Meanwhile, the flavor wave function of the other two 4-quark systems are simply $b\bar{b}s\bar{q}$ and $b\bar{b}s\bar{s}$, respectively.

Note, too, that the third component of the isospin, M_I , is fixed to be zero for simplicity since the Hamiltonian does not have a flavor-dependent interaction which can distinguish the third component of the isospin quantum number.

We are going to consider S -wave ground states with spin ranging from $S = 0$ to 2. Therefore, the spin wave functions, $\chi_{S, M_S}^{\sigma_i}$, are given by (M_S can be set to be equal to S without loss of generality):

$$\chi_{0,0}^{\sigma_{u_1}}(4) = \chi_{00}^{\sigma} \chi_{00}^{\sigma}, \quad (28)$$

$$\chi_{0,0}^{\sigma_{u_2}}(4) = \frac{1}{\sqrt{3}}(\chi_{11}^{\sigma} \chi_{1,-1}^{\sigma} - \chi_{10}^{\sigma} \chi_{10}^{\sigma} + \chi_{1,-1}^{\sigma} \chi_{11}^{\sigma}), \quad (29)$$

$$\begin{aligned} \chi_{0,0}^{\sigma_{u_3}}(4) = & \frac{1}{\sqrt{2}} \left(\left(\sqrt{\frac{2}{3}} \chi_{11}^{\sigma} \chi_{\frac{1}{2}, -\frac{1}{2}}^{\sigma} - \sqrt{\frac{1}{3}} \chi_{10}^{\sigma} \chi_{\frac{1}{2}, \frac{1}{2}}^{\sigma} \right) \chi_{\frac{1}{2}, -\frac{1}{2}}^{\sigma} \right. \\ & \left. - \left(\sqrt{\frac{1}{3}} \chi_{10}^{\sigma} \chi_{\frac{1}{2}, -\frac{1}{2}}^{\sigma} - \sqrt{\frac{2}{3}} \chi_{1,-1}^{\sigma} \chi_{\frac{1}{2}, \frac{1}{2}}^{\sigma} \right) \chi_{\frac{1}{2}, \frac{1}{2}}^{\sigma} \right), \quad (30) \end{aligned}$$

$$\chi_{0,0}^{\sigma_{u_4}}(4) = \frac{1}{\sqrt{2}}(\chi_{00}^{\sigma} \chi_{\frac{1}{2}, \frac{1}{2}}^{\sigma} \chi_{\frac{1}{2}, -\frac{1}{2}}^{\sigma} - \chi_{00}^{\sigma} \chi_{\frac{1}{2}, -\frac{1}{2}}^{\sigma} \chi_{\frac{1}{2}, \frac{1}{2}}^{\sigma}), \quad (31)$$

$$\chi_{1,1}^{\sigma_{w_1}}(4) = \chi_{00}^{\sigma} \chi_{11}^{\sigma}, \quad (32)$$

$$\chi_{1,1}^{\sigma_{w_2}}(4) = \chi_{11}^{\sigma} \chi_{00}^{\sigma}, \quad (33)$$

$$\chi_{1,1}^{\sigma_{w_3}}(4) = \frac{1}{\sqrt{2}}(\chi_{11}^{\sigma} \chi_{10}^{\sigma} - \chi_{10}^{\sigma} \chi_{11}^{\sigma}), \quad (34)$$

$$\begin{aligned} \chi_{1,1}^{\sigma_{w_4}}(4) = & \sqrt{\frac{3}{4}} \chi_{11}^{\sigma} \chi_{\frac{1}{2}, \frac{1}{2}}^{\sigma} \chi_{\frac{1}{2}, -\frac{1}{2}}^{\sigma} - \sqrt{\frac{1}{12}} \chi_{11}^{\sigma} \chi_{\frac{1}{2}, -\frac{1}{2}}^{\sigma} \chi_{\frac{1}{2}, \frac{1}{2}}^{\sigma} \\ & - \sqrt{\frac{1}{6}} \chi_{10}^{\sigma} \chi_{\frac{1}{2}, \frac{1}{2}}^{\sigma} \chi_{\frac{1}{2}, \frac{1}{2}}^{\sigma}, \quad (35) \end{aligned}$$

$$\chi_{1,1}^{\sigma_{w_5}}(4) = \left(\sqrt{\frac{2}{3}} \chi_{11}^{\sigma} \chi_{\frac{1}{2}, -\frac{1}{2}}^{\sigma} - \sqrt{\frac{1}{3}} \chi_{10}^{\sigma} \chi_{\frac{1}{2}, \frac{1}{2}}^{\sigma} \right) \chi_{\frac{1}{2}, \frac{1}{2}}^{\sigma}, \quad (36)$$

$$\chi_{1,1}^{\sigma_{w_6}}(4) = \chi_{00}^{\sigma} \chi_{\frac{1}{2}, \frac{1}{2}}^{\sigma} \chi_{\frac{1}{2}, \frac{1}{2}}^{\sigma}, \quad (37)$$

$$\chi_{2,2}^{\sigma_1}(4) = \chi_{11}^{\sigma} \chi_{11}^{\sigma}. \quad (38)$$

The superscripts u_1, \dots, u_4 and w_1, \dots, w_6 determine the spin wave function for each configuration of the $b\bar{b}q\bar{q}$ ($q = u, d, s$) tetraquark system, their specific values are shown in Table III. Furthermore, the expressions above are obtained by considering the coupling of two sub-clusters whose spin wave functions are given by trivial $SU(2)$ algebra, and the necessary basis reads as

$$\chi_{11}^{\sigma} = \chi_{\frac{1}{2}, \frac{1}{2}}^{\sigma} \chi_{\frac{1}{2}, \frac{1}{2}}^{\sigma}, \quad (39)$$

$$\chi_{1,-1}^{\sigma} = \chi_{\frac{1}{2}, -\frac{1}{2}}^{\sigma} \chi_{\frac{1}{2}, -\frac{1}{2}}^{\sigma}, \quad (40)$$

$$\chi_{10}^{\sigma} = \frac{1}{\sqrt{2}}(\chi_{\frac{1}{2}, \frac{1}{2}}^{\sigma} \chi_{\frac{1}{2}, -\frac{1}{2}}^{\sigma} + \chi_{\frac{1}{2}, -\frac{1}{2}}^{\sigma} \chi_{\frac{1}{2}, \frac{1}{2}}^{\sigma}), \quad (41)$$

$$\chi_{00}^{\sigma} = \frac{1}{\sqrt{2}}(\chi_{\frac{1}{2}, \frac{1}{2}}^{\sigma} \chi_{\frac{1}{2}, -\frac{1}{2}}^{\sigma} - \chi_{\frac{1}{2}, -\frac{1}{2}}^{\sigma} \chi_{\frac{1}{2}, \frac{1}{2}}^{\sigma}), \quad (42)$$

Among the different methods to solve the Schrödinger-like 4-body bound state equation, we use the Rayleigh-Ritz variational principle which is one of the most extended tools to solve eigenvalue problems because its

TABLE III. The values of the superscripts u_1, \dots, u_4 and w_1, \dots, w_6 that determine the spin wave function for each configuration of the $b\bar{b}q\bar{q}$ ($q = u, d, s$) tetraquark system.

	Di-meson	Diquark-antidiquark	K_1	K_2	K_3	K_4
u_1	1	3				
u_2	2	4				
u_3			5	7	9	11
u_4			6	8	10	12
w_1	1	4				
w_2	2	5				
w_3	3	6				
w_4			7	10	13	16
w_5			8	11	14	17
w_6			9	12	15	18

simplicity and flexibility. Moreover, we use the complex-range method and thus the spatial wave function is written as follows:

$$\psi_{LM_L}(\theta) = \left[\left[\phi_{n_1 l_1}(\vec{\rho} e^{i\theta}) \phi_{n_2 l_2}(\vec{\lambda} e^{i\theta}) \right]_l \phi_{n_3 l_3}(\vec{R} e^{i\theta}) \right]_{LM_L}, \quad (43)$$

where the internal Jacobi coordinates are defined as

$$\vec{\rho} = \vec{x}_1 - \vec{x}_2, \quad (44)$$

$$\vec{\lambda} = \vec{x}_3 - \vec{x}_4, \quad (45)$$

$$\vec{R} = \frac{m_1 \vec{x}_1 + m_2 \vec{x}_2}{m_1 + m_2} - \frac{m_3 \vec{x}_3 + m_4 \vec{x}_4}{m_3 + m_4}, \quad (46)$$

for the meson-meson configurations of panels 1(a) and (b); and as

$$\vec{\rho} = \vec{x}_1 - \vec{x}_3, \quad (47)$$

$$\vec{\lambda} = \vec{x}_2 - \vec{x}_4, \quad (48)$$

$$\vec{R} = \frac{m_1 \vec{x}_1 + m_3 \vec{x}_3}{m_1 + m_3} - \frac{m_2 \vec{x}_2 + m_4 \vec{x}_4}{m_2 + m_4}, \quad (49)$$

for the diquark-antidiquark structure of panel 1(c). The remaining K-type configurations shown in panels 1(d) to 1(g) are (i, j, k, l) take values according to the panels (d) to (g) of Fig. 1):

$$\vec{\rho} = \vec{x}_i - \vec{x}_j, \quad (50)$$

$$\vec{\lambda} = \vec{x}_k - \frac{m_i \vec{x}_i + m_j \vec{x}_j}{m_i + m_j}, \quad (51)$$

$$\vec{R} = \vec{x}_l - \frac{m_i \vec{x}_i + m_j \vec{x}_j + m_k \vec{x}_k}{m_i + m_j + m_k}. \quad (52)$$

It becomes obvious now that the center-of-mass kinetic term T_{CM} can be completely eliminated for a non-relativistic system defined in any of the above sets of relative coordinates.

A crucial aspect of the Rayleigh-Ritz variational method is the basis expansion of the trial wave function. We are going to use the Gaussian expansion method

(GEM) [70] in which each relative coordinate is expanded in terms of Gaussian basis functions whose sizes are taken in geometric progression. This method has proven to be very efficient on solving the bound-state problem of multi-quark systems [38] and the details on how the geometric progression is fixed can be found in, *e.g.*, Ref. [34]. Therefore, the form of the orbital wave functions, ϕ 's, in Eq. (43) is

$$\phi_{nlm}(\vec{r} e^{i\theta}) = N_{nl} (r e^{i\theta})^l e^{-\nu_n (r e^{i\theta})^2} Y_{lm}(\hat{r}). \quad (53)$$

Since only S -wave states of $b\bar{b}q\bar{q}$ tetraquarks are investigated in this work, no laborious Racah algebra is needed while computing matrix elements; the value of the spherical harmonic function is just a constant, *viz.* $Y_{00} = \sqrt{1/4\pi}$.

Finally, the complete wave-function that fulfills the Pauli principle is written as

$$\Psi_{JM_J, I, i, j, k}(\theta) = \left[[\psi_L(\theta) \chi_S^{\sigma_i}(4)]_{JM_J} \chi_I^{f_j} \chi_k^c \right]. \quad (54)$$

III. RESULTS

In the present calculation, we investigate all possible S -wave $b\bar{b}q\bar{q}$ ($q = u, d, s$) tetraquarks by taking into account di-meson, diquark-antidiquark and K-type configurations. In our approach, a $b\bar{b}q\bar{q}$ tetraquark state has positive parity assuming that the angular momenta l_1, l_2 and l_3 in Eq. (43) are all equal to zero. Accordingly, the total angular momentum, J , coincides with the total spin, S , and can take values of 0, 1 and 2. Besides, the value of isospin, I , can be either 0 or 1 considering the quark content of $b\bar{b}q\bar{q}$ system in the $SU(2)$ flavor symmetry; however, it is $I = 1/2$ for $b\bar{b}q\bar{s}$ and just 0 for $b\bar{b}s\bar{s}$.

Tables IV to XV list our calculated results of the lowest-lying $b\bar{b}q\bar{q}$ tetraquark states. The allowed meson-meson, diquark-antidiquark and K-type configurations are listed in the first column; when possible, the experimental value of the non-interacting meson-meson threshold is labeled in parentheses. Each channel is assigned an index in the second column, it reflects a particular combination of spin ($\chi_J^{\sigma_i}$), flavor ($\chi_I^{f_j}$) and color (χ_k^c) wave functions that are shown explicitly in the third column. The theoretical mass obtained in each channel is shown in the fourth column and the coupled result for each kind of configuration is presented in the last column. When a complete coupled-channels calculation is performed, last row of the table indicates the lowest-lying mass. When the CSM is used in the complete coupled-channels calculation, we show in Figs. 2 to 13, the distribution of complex eigen-energies and, therein, the obtained resonance states are indicated inside circles.

Let us proceed now to describe in detail our theoretical findings for each sector of $b\bar{b}q\bar{q}$ tetraquarks.

TABLE IV. Lowest-lying $b\bar{b}q\bar{q}$ tetraquark states with $I(J^P) = 0(0^+)$ calculated within the real range formulation of the chiral quark model. The allowed meson-meson, diquark-antidiquark and K-type configurations are listed in the first column; when possible, the experimental value of the non-interacting meson-meson threshold is labeled in parentheses. Each channel is assigned an index in the 2nd column, it reflects a particular combination of spin ($\chi_J^{\sigma_i}$), flavor ($\chi_I^{f_j}$) and color (χ_k^c) wave functions that are shown explicitly in the 3rd column. The theoretical mass obtained in each channel is shown in the 4th column and the coupled result for each kind of configuration is presented in the 5th column. When a complete coupled-channels calculation is performed, last row of the table indicates the lowest-lying mass. (unit: MeV).

Channel	Index	$\chi_J^{\sigma_i}; \chi_I^{f_j}; \chi_k^c$ [$i; j; k$]	M	Mixed
$(\eta_b\eta)^1(9848)$	1	[1; 1; 1]	10143	
$(\Upsilon\omega)^1(10242)$	2	[2; 1; 1]	10201	
$(B\bar{B})^1(10560)$	3	[1; 1; 1]	10556	
$(B^*\bar{B}^*)^1(10650)$	4	[2; 1; 1]	10638	10143
$(\eta_b\eta)^8$	5	[1; 1; 2]	10959	
$(\Upsilon\omega)^8$	6	[2; 1; 2]	10814	
$(B\bar{B})^8$	7	[1; 1; 2]	10680	
$(B^*\bar{B}^*)^8$	8	[2; 1; 2]	10666	10589
$(bq)(\bar{q}\bar{b})$	9	[3; 1; 3]	10774	
$(bq)(\bar{q}\bar{b})$	10	[3; 1; 4]	10729	
$(bq)^*(\bar{q}\bar{b})^*$	11	[4; 1; 3]	10829	
$(bq)^*(\bar{q}\bar{b})^*$	12	[4; 1; 4]	10708	10514
K_1	13	[5; 1; 5]	10817	
	14	[6; 1; 5]	10960	
	15	[5; 1; 6]	10538	
	16	[6; 1; 6]	10484	10483
K_3	17	[9; 1; 9]	10700	
	18	[10; 1; 9]	10722	
	19	[9; 1; 10]	10825	
	20	[10; 1; 10]	10767	10507
Complete coupled-channels:				10143

A. The $b\bar{b}q\bar{q}$ ($q = u, d$) tetraquarks

Each iso-scalar and -vector sectors with total spin and parity $J^P = 0^+, 1^+$ and 2^+ shall be discussed individually below. Particularly, due to symmetry properties of the Hamiltonian with respect to the K-type configurations of $b\bar{b}q\bar{q}$ tetraquarks, only K_1 and K_3 arrangements are sufficient to consider.

The $I(J^P) = 0(0^+)$ sector: Four meson-meson channels, $\eta_b\eta$, $\Upsilon\omega$, $B\bar{B}$ and $B^*\bar{B}^*$ in both color-singlet and hidden-color configurations, four diquark-antidiquark channels, along with K-type configurations

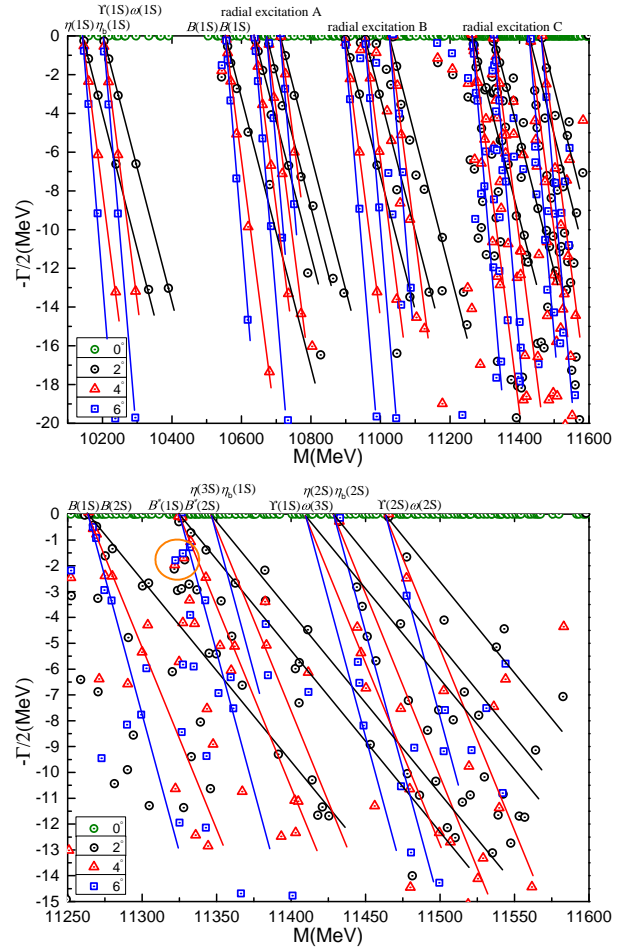


FIG. 2. *Top panel:* The complete coupled-channels calculation of $b\bar{b}q\bar{q}$ tetraquark system with $I(J^P) = 0(0^+)$ quantum numbers. *Bottom panel:* Enlarged top panel, with real values of energy ranging from 11.25 GeV to 11.60 GeV. We use the complex-scaling method of the chiral quark model varying θ from 0° to 6° .

are individually studied in Table IV. One can see that the formation of a bound state is not possible in each single channel calculation. The four singlet-color meson-meson states are located above their thresholds with masses at 10.14 GeV, 10.20 GeV, 10.55 GeV and 10.64 GeV, respectively. The other tetraquark configurations: hidden-color meson-meson, diquark-antidiquark, and K-type channels, present states in an energy region which ranges from 10.70 GeV to 10.96 GeV. After a coupled-channels calculation among each type of configuration is performed, the lowest mass is around 10.5 GeV for the three exotic structures hidden-color, diquark-antidiquark and K-type. However, the lowest mass in singlet-color coupled-channels calculation remains at the $\eta_b\eta$ theoretical threshold value of 10.14 GeV. This result also holds for the fully coupled-channels computation in a real-range investigation.

In a further step, a complete coupled-channels calculation is performed using the complex-range method and its

output is shown in Fig. 2. Therein, with a rotated angle ranging from 0° to 6° , the scattering states of two mesons are well presented within an interval of 10.10 – 11.60 GeV. In particular, apart from the three lower scattering states, $\eta_b(1S)\eta(1S)$, $\Upsilon(1S)\omega(1S)$ and $B(1S)\bar{B}(1S)$, presented in the top panel, the other dimeson channels, listed in Table IV, along with their radial excitations are generally located in the regions of A , B and C of Fig. 2, respectively. In particular, there are three channels, $B^*(1S)\bar{B}^*(1S)$, $\eta_b(2S)\eta(1S)$ and $\Upsilon(2S)\omega(1S)$ in the region A , another three in B which are $\eta_b(1S)\eta(2S)$, $\Upsilon(1S)\omega(2S)$ and $\Upsilon(3S)\omega(1S)$; and six radial excitation channels of region C are clearly shown in the bottom panel of Fig. 2. Therein, two narrow resonance poles are obtained above the $B(1S)\bar{B}(2S)$ threshold lines. Their calculated complex energies, which are denoted as $M+i\Gamma$, are $11322+i3.9$ MeV and $11328+i3.4$ MeV, respectively. The dominant decay channel of these almost degenerate resonances could be the $B(1S)\bar{B}(2S)$ state.

The $I(J^P) = 0(1^+)$ sector: There are 26 channels in this sector which includes five color-singlet meson-meson configurations, another five in the hidden-color meson-meson ones, four more in diquark-antidiquark arrangement, and 12 K-type configurations. Table V shows the obtained masses in each channels which are always above the lowest meson-meson threshold. The five di-meson structures in color-singlet configuration have masses within an energy region of 10.15 – 10.60 GeV. Furthermore, masses of the hidden-color $(b\bar{b})(q\bar{q})$ configurations are ~ 10.90 GeV and ~ 10.67 GeV for the $(q\bar{b})(b\bar{q})$ ones, respectively; diquark-antidiquark channels are characterized with masses ranging from 10.70 GeV to 10.81 GeV; and, for the K-type configurations, each calculated channel presents a mass lying in an interval of 10.48 – 10.92 GeV.

If one considers the coupling between channels of the same kind of tetraquark configuration, the lowest masses are located at ~ 10.5 GeV for the exotic structures hidden-color, diquark-antidiquark and K-type. However, the induced binding due to coupling is extremely weak in color-singlet di-meson case and the lowest mass remains at 10.15 GeV of the $\eta_b\omega$ theoretical threshold value. Furthermore, the same result is also obtained in a real-range calculation when all of the channels listed in Table V are considered. Hence, bound state is excluded.

Figure 3 presents the calculated results of fully coupled-channels case with the complex-range method employed. The general distributions of complex energies of $b\bar{b}q\bar{q}$ system are presented in the top panel of Fig. 3, whose energy range is from 10.10 to 11.30 GeV. Within a rotated angle ranging from 0° to 6° , the scattering nature of $\eta_b\omega$, $\Upsilon\eta$, $\Upsilon\omega$ and $B^{(*)}\bar{B}^{(*)}$ are clearly shown. However, four stable poles are obtained against the variation of rotated angle θ . Their computed masses(M) and widths(Γ) read $10584+i1.6$ MeV, $11073+i1.8$ MeV, $11209+i2.8$ MeV and $11272+i5.0$ MeV, respectively.

In order to have a better analysis of these resonances, two regions of dense radial excitations whose energy in-

TABLE V. Lowest-lying $b\bar{b}q\bar{q}$ tetraquark states with $I(J^P) = 0(1^+)$ calculated within the real range formulation of the chiral quark model. The results are similarly organized as those in Table IV. (unit: MeV).

Channel	Index	$\chi_J^{\sigma_i}; \chi_I^{f_j}; \chi_k^c$ [$i; j; k$]	M	Mixed
$(\eta_b\omega)^1(10082)$	1	[1; 1; 1]	10150	
$(\Upsilon\eta)^1(10008)$	2	[2; 1; 1]	10194	
$(\Upsilon\omega)^1(10242)$	3	[3; 1; 1]	10201	
$(B\bar{B}^*)^1(10605)$	4	[1; 1; 1]	10597	
$(B^*\bar{B}^*)^1(10650)$	5	[3; 1; 1]	10638	10150
$(\eta_b\omega)^8$	6	[1; 1; 2]	10831	
$(\Upsilon\eta)^8$	7	[2; 1; 2]	10960	
$(\Upsilon\omega)^8$	8	[3; 1; 2]	10823	
$(B\bar{B}^*)^8$	9	[1; 1; 2]	10681	
$(B^*\bar{B}^*)^8$	10	[3; 1; 2]	10667	10587
$(bq)(\bar{q}\bar{b})^*$	11	[4; 1; 3]	10788	
$(bq)(\bar{q}\bar{b})^*$	12	[4; 1; 4]	10807	
$(bq)^*(\bar{q}\bar{b})^*$	13	[6; 1; 3]	10725	
$(bq)^*(\bar{q}\bar{b})^*$	14	[6; 1; 4]	10705	10524
K_1	15	[7; 1; 5]	10922	
	16	[8; 1; 5]	10878	
	17	[9; 1; 5]	10835	
	18	[7; 1; 6]	10536	
	19	[8; 1; 6]	10537	
	20	[9; 1; 6]	10487	10487
K_3	21	[13; 1; 9]	10718	
	22	[14; 1; 9]	10677	
	23	[15; 1; 9]	10717	
	24	[13; 1; 10]	10813	
	25	[14; 1; 10]	10744	
	26	[15; 1; 10]	10780	10511
Complete coupled-channels:				10150

tervals are 10.55 – 10.85 GeV and 10.90 – 11.10 GeV, respectively, are plotted in the middle and bottom panels of Fig. 3. From the middle panel, we could find that one resonance pole is quite close to the $B(1S)\bar{B}^*(1S)$ threshold line(s). Apparently, this resonance with $I(J^P) = 0(1^+)$ has a mass similar to the the exotic state $Z_b(10610)$ but cannot be assigned because the experimental candidate has isospin one.

Additionally, in the high energy region of the bottom panel, the radial excited states of $\eta_b\omega$, $\Upsilon\eta$ and $\Upsilon\omega$ are generally presented. Moreover, there is also an indication of a resonance above the $\Upsilon(3S)\omega(1S)$ threshold, and this pole is located at $11073+i1.8$ MeV. A similar conclusion is obtained at around 11.2 GeV, therein, two resonances

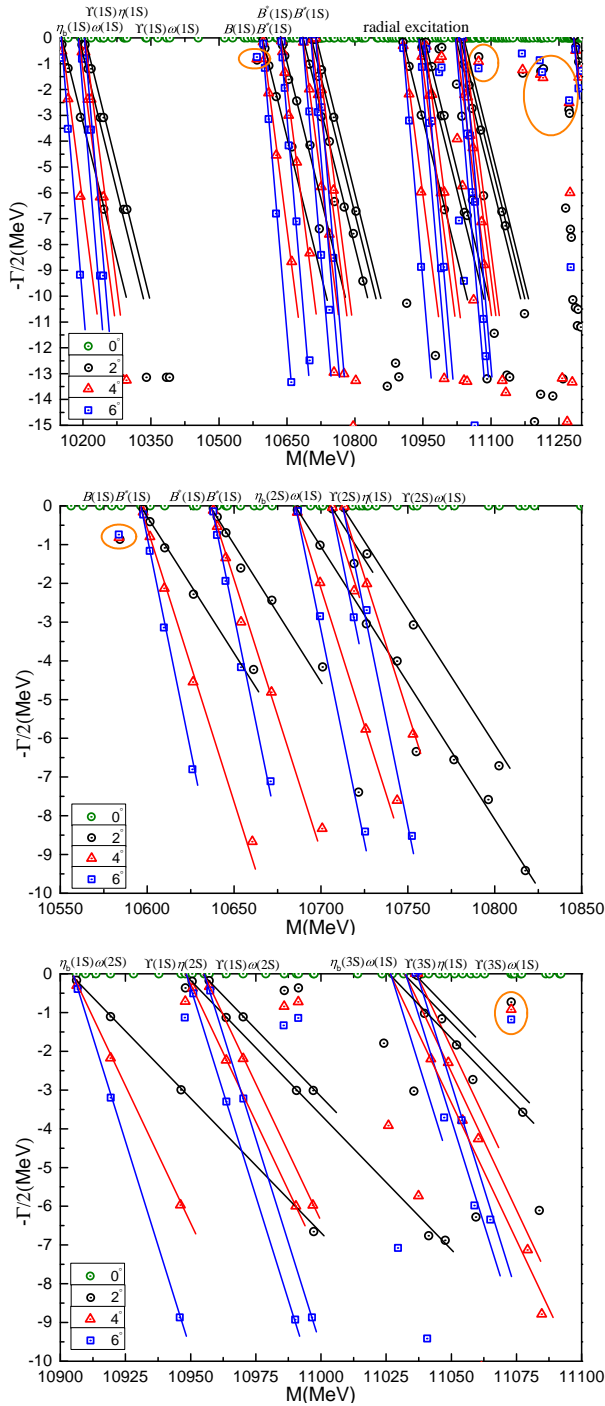


FIG. 3. The complete coupled-channels calculation of $b\bar{b}q\bar{q}$ tetraquark system with $I(J^P) = 0(1^+)$. Particularly, middle and bottom panels are the enlarged parts of dense energy region from 10.55 GeV to 11.10 GeV.

with $11209 + i2.8$ MeV and $11272 + i5.0$ MeV are clearly shown in the big circle of top panel. The $\Upsilon(3S)\omega(1S)$ should be the dominant decay channel of these three resonances and they are expected to be identified in the future high energy experiments with mass ~ 11.2 GeV

TABLE VI. Lowest-lying $b\bar{b}q\bar{q}$ tetraquark states with $I(J^P) = 0(2^+)$ calculated within the real range formulation of the chiral quark model. The results are similarly organized as those in Table IV. (unit: MeV).

Channel	Index	$\chi_I^{\sigma_i}; \chi_I^{f_j}; \chi_k^c$ [$i; j; k$]	M	Mixed
$(\Upsilon\omega)^1(10242)$	1	[1; 1; 1]	10201	
$(B^*\bar{B}^*)^1(10650)$	2	[1; 1; 1]	10626	10201
$(\Upsilon\omega)^8$	3	[1; 1; 2]	10840	
$(B^*\bar{B}^*)^8$	4	[1; 1; 2]	10670	10604
$(bq)^*(\bar{q}\bar{b})^*$	5	[1; 1; 3]	10756	
$(bq)^*(\bar{q}\bar{b})^*$	6	[1; 1; 4]	10699	10544
K_1	7	[1; 1; 5]	10845	
	8	[1; 1; 6]	10538	10538
K_3	9	[1; 1; 9]	10690	
	10	[1; 1; 10]	10743	10543
Complete coupled-channels:				10201

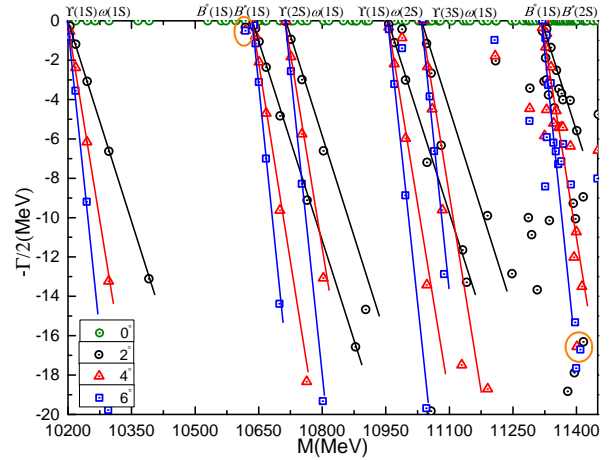


FIG. 4. The complete coupled-channels calculation of the $b\bar{b}q\bar{q}$ tetraquark system with $I(J^P) = 0(2^+)$ quantum numbers. We use the complex-scaling method of the chiral quark model varying θ from 0° to 6° .

and quantum numbers $I(J^P) = 0(1^+)$.

The $I(J^P) = 0(2^+)$ state: Table VI shows that two meson-meson structures, $\Upsilon\omega$ and $B^*\bar{B}^*$ (in both color-singlet and hidden-color configurations), one $(bq)^*(\bar{q}\bar{b})^*$ diquark-antidiquark arrangement and four K-type configurations contribute to the $I(J^P) = 0(2^+)$ state.

Firstly, in each single channel calculation, a $B^*\bar{B}^*$ bound state, which binding energy is -12 MeV, is found in its color-singlet channel, and the modified mass is 10638 MeV. Although this value is quite compatible with $Z_b(10650)$ mass, a conclusion can not be drawn herein

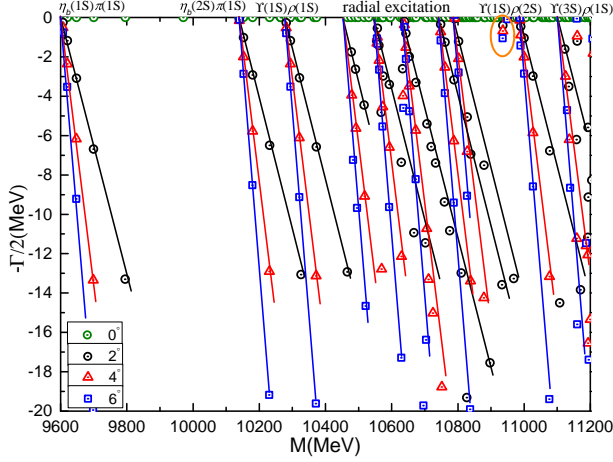


FIG. 5. The complete coupled-channels calculation of the $bb\bar{q}\bar{q}$ tetraquark system with $I(J^P) = 1(0^+)$ quantum numbers. We use the complex-scaling method of the chiral quark model varying θ from 0° to 6° .

for coupling effect is not considered temporarily and the spin-parity conflicts with 1^+ experimentally. Meanwhile, the lowest channel, $\Upsilon\omega$, is of scattering nature with theoretical mass at 10.20 GeV. The other exotic configurations: hidden-color dimeson, diquark-antidiquark and K-type, are generally located above 10.7 GeV, except for one K_1 channel with a calculated mass at 10538 MeV.

When real-range coupled-channel computations are performed in each kind of structure, firstly, in the color-singlet channels, the lowest energy remains at $\Upsilon\omega$ threshold value of 10.20 GeV (this result is unchanged even in a fully coupled case), and masses of the other four multi-quark arrangements are around 10.54 GeV.

In a further step, Fig. 4 shows the calculated results obtained in a complex-range investigation. The $\Upsilon\omega$ and $B^*\bar{B}^*$ thresholds, considering each meson in both ground and radial excitation, are well presented within an energy interval of 10.20 – 11.50 GeV. Moreover, two resonance states are obtained (circled in the figure) at $10618 + i1.0$ MeV and $11416 + i32.6$ MeV, respectively. The narrow state is quite close to $B^*(1S)\bar{B}^*(1S)$ threshold line, whereas the wide resonance is located at the $B^*(1S)\bar{B}^*(2S)$ threshold line.

The $I(J^P) = 1(0^+)$ sector: Table VII lists our results for the isovector $bb\bar{q}\bar{q}$ tetraquark with spin-parity $J^P = 0^+$. As in the case of the $I(J^P) = 0(0^+)$ sector, 20 channels are under investigation and no one shows a bound state, except the color-singlet channel $B^*\bar{B}^*$ with a very small binding energy $E_b = -4$ MeV. Apart from the lowest channel $\eta_b\pi$ ($M = 9603$), masses of color-singlet meson-meson configurations are located at 10.28 – 10.63 GeV. The other color configurations are in a mass region between 10.57 GeV and 10.87 GeV, note however that K_1 channel has a mass of 10.35 GeV. Furthermore, in each exotic configuration's coupled-channel computation, the lowest mass tends to 10.35 GeV, and

TABLE VII. Lowest-lying $bb\bar{q}\bar{q}$ tetraquark states with $I(J^P) = 1(0^+)$ calculated within the real range formulation of the chiral quark model. The results are similarly organized as those in Table IV. (unit: MeV).

Channel	Index	$\chi_{J^i}^{\sigma_i}; \chi_{I^j}^{f_j}; \chi_k^c$ [$i; j; k$]	M	Mixed
$(\eta_b\pi)^1(9440)$	1	[1; 1; 1]	9603	
$(\Upsilon\rho)^1(10230)$	2	[2; 1; 1]	10277	
$(B\bar{B})^1(10560)$	3	[1; 1; 1]	10556	
$(B^*\bar{B}^*)^1(10650)$	4	[2; 1; 1]	10634	9603
$(\eta_b\pi)^8$	5	[1; 1; 2]	10830	
$(\Upsilon\rho)^8$	6	[2; 1; 2]	10875	
$(B\bar{B})^8$	7	[1; 1; 2]	10680	
$(B^*\bar{B}^*)^8$	8	[2; 1; 2]	10601	10455
$(bq)(\bar{q}\bar{b})$	9	[3; 1; 3]	10774	
$(bq)(\bar{q}\bar{b})$	10	[3; 1; 4]	10740	
$(bq)^*(\bar{q}\bar{b})^*$	11	[4; 1; 3]	10729	
$(bq)^*(\bar{q}\bar{b})^*$	12	[4; 1; 4]	10622	10383
K_1	13	[5; 1; 5]	10868	
	14	[6; 1; 5]	10832	
	15	[5; 1; 6]	10570	
	16	[6; 1; 6]	10349	10348
K_3	17	[9; 1; 9]	10607	
	18	[10; 1; 9]	10722	
	19	[9; 1; 10]	10726	
	20	[10; 1; 10]	10767	10371
Complete coupled-channels:				9603

the scattering state of $\eta_b\pi$ at 9603 MeV remains unchanged in various analysis of this kind.

The complete coupled-channels calculation has been also extended to the complex-range. Figure 5 shows the distribution of complex energies within an energy range 9.6 – 11.2 GeV. The scattering nature of $\eta_b\pi$, $\Upsilon\rho$ and $B^{(*)}\bar{B}^{(*)}$, both in ground and radial excitation states, is clearly presented. In particular, there are five scattering states, $\eta_b(3S)\pi(1S)$, $B(1S)\bar{B}(1S)$, $B^*(1S)\bar{B}^*(1S)$, $\eta_b(1S)\pi(2S)$ and $\Upsilon(2S)\rho(1S)$, located in an energy region from 10.4 GeV to 10.9 GeV. With respect to the shallow $B^*\bar{B}^*$ bound state, whose mass is 10634 MeV, found in a color-singlet channel calculation, it disappears in the complete coupled-channel situation. Besides, one narrow resonance circled in Fig. 5 is obtained with a complex energy of $10935 + i1.4$ MeV. This pole locates between the threshold lines of $\Upsilon(2S)\rho(1S)$ and $\Upsilon(1S)\rho(2S)$, hence the dominate decay channel should be $\Upsilon(2S)\rho(1S)$.

The $I(J^P) = 1(1^+)$ sector: The numerical analysis of this case is quite similar to the $I(J^P) = 0(1^+)$ because 26 channels must be also explored. From Table VIII,

TABLE VIII. Lowest-lying $b\bar{b}q\bar{q}$ tetraquark states with $I(J^P) = 1(1^+)$ calculated within the real range formulation of the chiral quark model. The results are similarly organized as those in Table IV. (unit: MeV).

Channel	Index	$\chi_{J^i}^{\sigma^i}; \chi_{I^j}^{f^j}; \chi_k^c$ [$i; j; k$]	M	Mixed
$(\eta_b\rho)^1(10070)$	1	[1; 1; 1]	10226	
$(\Upsilon\pi)^1(9600)$	2	[2; 1; 1]	9654	
$(\Upsilon\rho)^1(10230)$	3	[3; 1; 1]	10277	
$(B\bar{B}^*)^1(10605)$	4	[1; 1; 1]	10597	
$(B^*\bar{B}^*)^1(10650)$	5	[3; 1; 1]	10636	9654
$(\eta_b\rho)^8$	6	[1; 1; 2]	10890	
$(\Upsilon\pi)^8$	7	[2; 1; 2]	10830	
$(\Upsilon\rho)^8$	8	[3; 1; 2]	10883	
$(B\bar{B}^*)^8$	9	[1; 1; 2]	10681	
$(B^*\bar{B}^*)^8$	10	[3; 1; 2]	10637	10518
$(bq)(\bar{q}\bar{b})^*$	11	[4; 1; 3]	10788	
$(bq)^*(\bar{q}\bar{b})$	12	[4; 1; 4]	10762	
$(bq)^*(\bar{q}\bar{b})^*$	13	[6; 1; 3]	10725	
$(bq)^*(\bar{q}\bar{b})^*$	14	[6; 1; 4]	10664	10461
K_1	15	[7; 1; 5]	10848	
	16	[8; 1; 5]	10862	
	17	[9; 1; 5]	10884	
	18	[7; 1; 6]	10471	
	19	[8; 1; 6]	10525	
	20	[9; 1; 6]	10519	10400
K_3	21	[13; 1; 9]	10644	
	22	[14; 1; 9]	10705	
	23	[15; 1; 9]	10717	
	24	[13; 1; 10]	10730	
	25	[14; 1; 10]	10778	
	26	[15; 1; 10]	10780	10406
Complete coupled-channels:			9654	

we could find that the $B^*\bar{B}^*$ color-singlet channel is still weakly bound with $E_b = -2$ MeV, then the modified mass is 10648 MeV, and the other meson-meson configurations in this channel are all of scattering nature. Accordingly, the $Z_b(10650)$ could be identified as a $B^*\bar{B}^*$ shallow bound state. However, this state is quite unstable, and scattered in a complete coupled-channels study that is discussed in the next paragraph. Meanwhile, the single channel masses of exotic structures are in a region of 10.47 – 10.89 GeV, and coupled-channel mechanisms help little in pushing down the lowest masses, being all close to 10.4 GeV.

In a complex-range investigation of the complete coupled-channel calculation, where the rotated angle θ

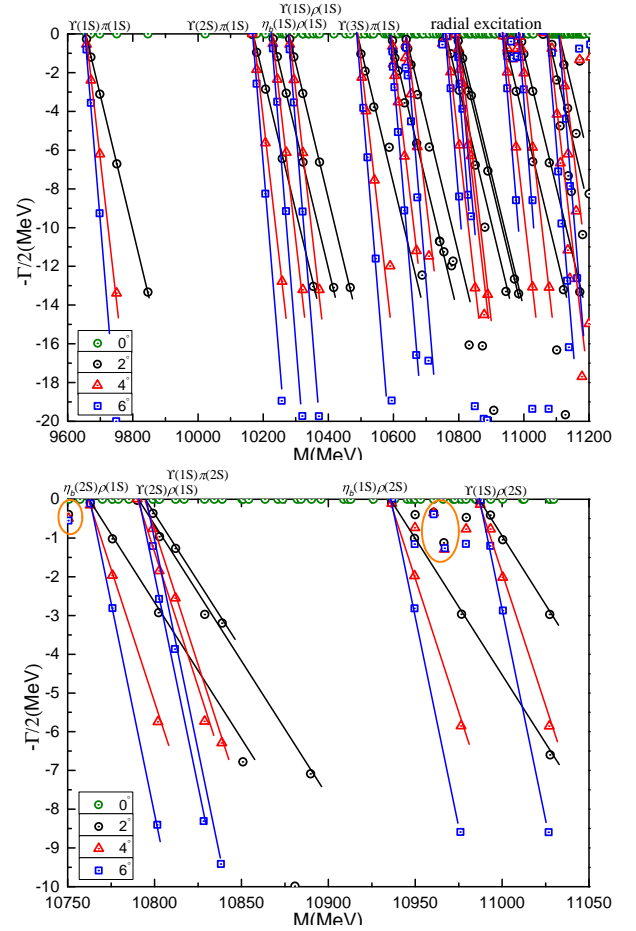


FIG. 6. *Top panel:* The complete coupled-channels calculation of the $b\bar{b}q\bar{q}$ tetraquark system with $I(J^P) = 1(1^+)$ quantum numbers. *Bottom panel:* Enlarged top panel, with real values of energy ranging from 10.75 GeV to 11.05 GeV. We use the complex-scaling method of the chiral quark model varying θ from 0° to 6° .

is still varied from 0° to 6° , the complex energies are presented in Fig. 6. In particular, within 9.6 – 11.2 GeV, the scattering states of $\Upsilon\pi$, $\Upsilon\rho$, $\eta_b\rho$ and $B^{(*)}\bar{B}^{(*)}$ are generally shown in the top panel. As mentioned above, it seems that no stable pole is obtained; in particular, the previously obtained $B^*\bar{B}^*$ shallow bound-state is unavailable. However, due to a dense distribution of radial excitation states in the energy region 10.75 – 11.05 GeV, an enlarged part is plotted in the bottom panel of Fig. 6. Therein, one could find three stable resonance poles. The calculated masses and widths read $10750 + i1.0$ MeV, $10960 + i0.7$ MeV and $10967 + i2.6$ MeV, respectively. Besides, according to their distributions, the dominant channel of the lowest resonance should be $B^*(1S)\bar{B}^*(1S)$ and the other two should be $\eta_b(1S)\rho(2S)$.

The $I(J^P) = 1(2^+)$ sector: The real- and complex-range results for the highest spin and isospin $b\bar{b}q\bar{q}$ channel are shown in Table IX and Fig. 7, respectively. The $\Upsilon\rho$ and $B^*\bar{B}^*$ cases are both scattering states. Further-

TABLE IX. Lowest-lying $b\bar{b}q\bar{q}$ tetraquark states with $I(J^P) = 1(2^+)$ calculated within the real range formulation of the chiral quark model. The results are similarly organized as those in Table IV. (unit: MeV).

Channel	Index	$\chi_{J^i}^{\sigma^i}; \chi_{I^j}^{f^j}; \chi_k^c$ [$i; j; k$]	M	Mixed
$(\Upsilon\rho)^1(10230)$	1	[1; 1; 1]	10277	
$(B^*\bar{B}^*)^1(10650)$	2	[1; 1; 1]	10638	10277
$(\Upsilon\rho)^8$	3	[1; 1; 2]	10898	
$(B^*\bar{B}^*)^8$	4	[1; 1; 2]	10698	10636
$(bq)^*(\bar{q}\bar{b})^*$	5	[1; 1; 3]	10802	
$(bq)^*(\bar{q}\bar{b})^*$	6	[1; 1; 4]	10737	10576
K_1	7	[1; 1; 5]	10893	
	8	[1; 1; 6]	10570	10570
K_3	9	[1; 1; 9]	10731	
	10	[1; 1; 10]	10794	10575
Complete coupled-channels:				10277

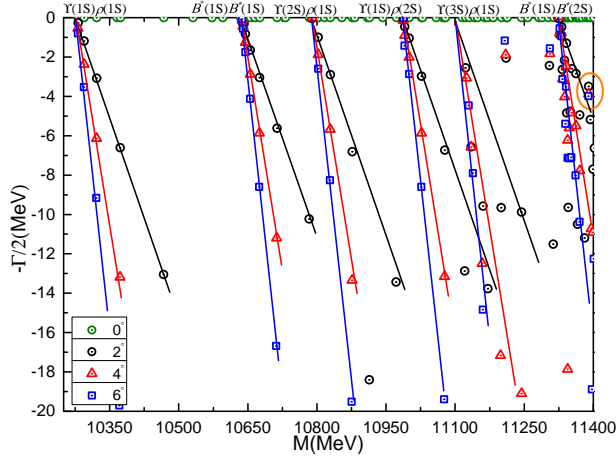


FIG. 7. The complete coupled-channels calculation of the $b\bar{b}q\bar{q}$ tetraquark system with $I(J^P) = 1(2^+)$ quantum numbers. We use the complex-scaling method of the chiral quark model varying θ from 0° to 6° .

more, those belonging to the hidden-color meson-meson, diquark-antidiquark and K-type configurations are generally located in the energy range 10.6 – 10.9 GeV. In the coupled-channel calculation of each quark-arrangement configuration, the masses are ~ 10.57 GeV, and the scattering nature of the lowest channel $\Upsilon\rho$ remains at 10277 MeV.

In Fig. 7, where a fully coupled-channel calculation in complex-range is performed, the distributions of complex energies of $\Upsilon\rho$ and $B^*\bar{B}^*$ are well presented. Moreover, a resonance state is found with mass and decay width

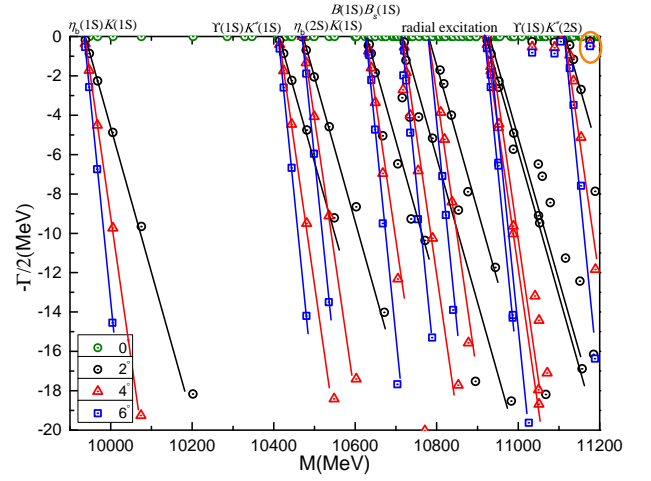


FIG. 8. The complete coupled-channels calculation of the $b\bar{b}u\bar{s}$ tetraquark system with $I(J^P) = \frac{1}{2}(0^+)$ quantum numbers. We use the complex-scaling method of the chiral quark model varying θ from 0° to 6° .

equal to $11390 + i7.8$ MeV; obviously, the $B^*(1S)\bar{B}^*(2S)$ should be its dominant channel.

B. The $b\bar{b}u\bar{s}$ tetraquarks

A natural continuation of the investigation performed above is the analysis of the $b\bar{b}u\bar{s}$ tetraquark system with spin-parity $J^P = 0^+, 1^+$ and 2^+ , and isospin $I = \frac{1}{2}$. A similar situation that the one discussed in the hidden-charm tetraquarks with strangeness [37] is found for the $b\bar{b}u\bar{s}$ tetraquarks. In summary, several narrow resonances whose masses are around 11.1 GeV are obtained, and further details can be found below.

The $I(J^P) = \frac{1}{2}(0^+)$ sector: Table X summarizes all contributing channels, they are 28 and include meson-meson, diquark-antidiquark and K-type structures. The color-singlet channels, which include $\eta_b K$, ΥK^* and $B^{(*)}B_s^{(*)}$, are all of scattering nature. Namely, their masses are just located at the values of corresponding theoretical thresholds. Besides, the remaining channels of hidden-color, diquark-antidiquark and K-type configurations are generally located in the interval 10.6 – 10.9 GeV.

If a coupled-channel calculation is performed in each individual configuration, the lowest masses of exotic configurations are close to 10.56 GeV, except for hidden-color channels which is located at 10.65 GeV. Meanwhile, the coupled mass of color-singlet channels is still at the $\eta_b K$ theoretical threshold value 9935 MeV, and this fact is not changed even in a complete coupled-channel calculation in real-range formulation.

When a fully coupled-channel calculation is performed in complex-range, Fig. 8 shows the obtained results. Therein, with an energy interval 9.0 – 11.2 GeV, the scattering nature of $\eta_b K$, ΥK^* and $B^{(*)}B_s^{(*)}$ both in ground

TABLE X. Lowest-lying $b\bar{b}u\bar{s}$ tetraquark states with $I(J^P) = \frac{1}{2}(0^+)$ calculated within the real range formulation of the chiral quark model. The results are similarly organized as those in Table IV. (unit: MeV).

Channel	Index	$\chi_{J^i}^{\sigma_i}; \chi_{I^j}^{f_j}; \chi_k^c$ [$i; j; k$]	M	Mixed
$(\eta_b K)^1(9794)$	1	[1; 2; 1]	9935	
$(\Upsilon K^*)^1(10352)$	2	[2; 2; 1]	10412	
$(BB_s)^1(10647)$	3	[1; 2; 1]	10633	
$(B^* B_s)^1(10740)$	4	[2; 2; 1]	10719	9935
$(\eta_b K)^8$	5	[1; 2; 2]	10963	
$(\Upsilon K^*)^8$	6	[2; 2; 2]	10978	
$(BB_s)^8$	7	[1; 2; 2]	10838	
$(B^* B_s^*)^8$	8	[2; 2; 2]	10776	10652
$(bu)(\bar{s}\bar{b})$	9	[3; 2; 3]	10875	
$(bu)(\bar{s}\bar{b})^*$	10	[4; 2; 3]	10853	
$(bu)^*(\bar{s}\bar{b})$	11	[3; 2; 4]	10844	
$(bu)^*(\bar{s}\bar{b})^*$	12	[4; 2; 4]	10757	10572
K_1	13	[5; 2; 5]	10970	
	14	[6; 2; 5]	10962	
	15	[5; 2; 6]	10701	
	16	[6; 2; 6]	10540	10539
K_2	17	[7; 2; 7]	10696	
	18	[8; 2; 7]	10533	
	19	[7; 2; 8]	10970	
	20	[8; 2; 8]	10961	10533
K_3	21	[9; 2; 9]	10742	
	22	[10; 2; 9]	10836	
	23	[9; 2; 10]	10839	
	24	[10; 2; 10]	10867	10562
K_4	25	[11; 2; 11]	10751	
	26	[12; 2; 11]	10844	
	27	[11; 2; 12]	10842	
	28	[12; 2; 12]	10870	10561
Complete coupled-channels:			9935	

and radial excitation states is clearly presented. Besides, one quite narrow resonance is found and we circle it above the $\Upsilon(1S)K^*(2S)$ threshold line(s); the calculated complex energy is $11176 + i0.8$ MeV and it should be stable against meson-meson strong decay processes.

The $I(J^P) = \frac{1}{2}(1^+)$ sector: 42 channels shown in Table XI are under investigation; namely, six meson-meson channels in both color-singlet and hidden-color configurations, six diquark-antidiquark structures, and 24 K-type arrangements. Firstly, in the single-channel calculation, no bound state is obtained. The lowest one

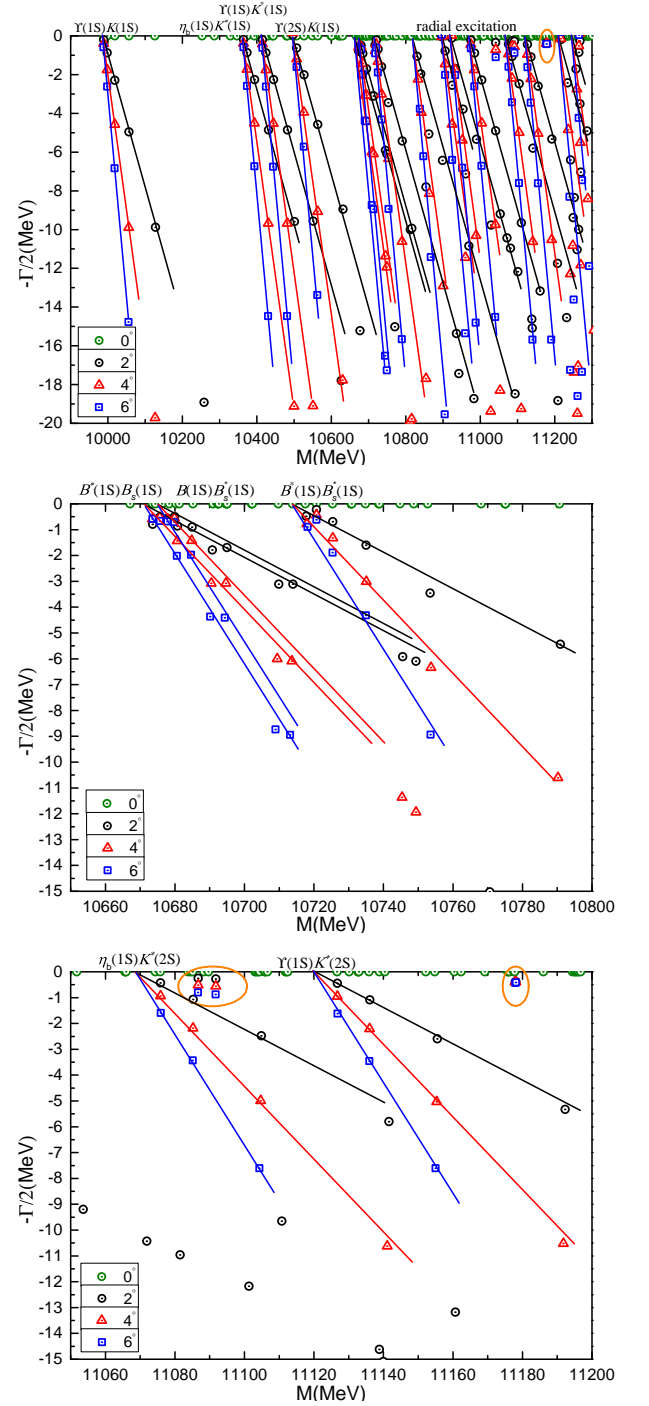


FIG. 9. The complete coupled-channels calculation of the $b\bar{b}u\bar{s}$ tetraquark system with $I(J^P) = \frac{1}{2}(1^+)$ quantum numbers. Particularly, middle and bottom panels are the enlarged parts of dense energy region from 10.65 GeV to 11.20 GeV.

is ΥK scattering state with mass at 9986 MeV, and the other color-singlet channels are generally located in an interval 10.3 – 10.7 GeV. Besides, masses of exotic configurations distribute from 10.6 GeV to 10.9 GeV. Although the coupled mass in hidden-color, diquark-antidiquark, and K-type configurations tends to 10.59

TABLE XI. Lowest-lying $b\bar{b}u\bar{s}$ tetraquark states with $I(J^P) = \frac{1}{2}(1^+)$ calculated within the real range formulation of the chiral quark model. The results are similarly organized as those in Table IV. (unit: MeV).

Channel	Index	$\chi_J^{\sigma_i}; \chi_I^{f_j}; \chi_k^c$ [$i; j; k$]	M	Mixed	Channel	Index	$\chi_J^{\sigma_i}; \chi_I^{f_j}; \chi_k^c$ [$i; j; k$]	M	Mixed
$(\eta_b K^*)^1(10192)$	1	[1; 2; 1]	10361		K_1	19	[7; 2; 5]	10969	
$(\Upsilon K)^1(9954)$	2	[2; 2; 1]	9986			20	[8; 2; 5]	10972	
$(\Upsilon K^*)^1(10352)$	3	[3; 2; 1]	10412			21	[9; 2; 5]	10986	
$(B^* B_s)^1(10692)$	4	[1; 2; 1]	10674			22	[7; 2; 6]	10635	
$(B B_s^*)^1(10695)$	5	[2; 2; 1]	10678			23	[8; 2; 6]	10670	
$(B^* B_s^*)^1(10740)$	6	[3; 2; 1]	10719	9986		24	[9; 2; 6]	10650	10591
$(\eta_b K^*)^8$	7	[1; 2; 2]	10992		K_2	25	[10; 2; 7]	10629	
$(\Upsilon K)^8$	8	[2; 2; 2]	10964			26	[11; 2; 7]	10665	
$(\Upsilon K^*)^8$	9	[3; 2; 2]	10985			27	[12; 2; 7]	10645	
$(B^* B_s)^8$	10	[1; 2; 2]	10840			28	[10; 2; 8]	10966	
$(B B_s^*)^8$	11	[2; 2; 2]	10839			29	[11; 2; 8]	10974	
$(B^* B_s^*)^8$	12	[3; 2; 2]	10801	10675		30	[12; 2; 8]	10986	10584
$(bu)(\bar{s}\bar{b})^*$	13	[4; 2; 3]	10888		K_3	31	[13; 2; 9]	10773	
$(bu)(\bar{s}\bar{b})^*$	14	[5; 2; 3]	10889			32	[14; 2; 9]	10809	
$(bu)^*(\bar{s}\bar{b})$	15	[6; 2; 3]	10866			33	[15; 2; 9]	10831	
$(bu)^*(\bar{s}\bar{b})$	16	[4; 2; 4]	10841			34	[13; 2; 10]	10839	
$(bu)^*(\bar{s}\bar{b})^*$	17	[5; 2; 4]	10840			35	[14; 2; 10]	10868	
$(bu)^*(\bar{s}\bar{b})^*$	18	[6; 2; 4]	10787	10600		36	[15; 2; 10]	10881	10592
					K_4	37	[16; 2; 11]	10783	
						38	[17; 2; 11]	10815	
						39	[18; 2; 11]	10840	
						40	[16; 2; 12]	10844	
						41	[17; 2; 12]	10870	
						42	[18; 2; 12]	10882	10596
Complete coupled-channels:									9986

GeV, this strong coupling effect does not hold for color-singlet channels study, and the lowest mass remains at ΥK threshold value.

Fig. 9 shows our findings using the complex-range method to the complete coupled-channel calculation. Therein, in the top panel, the scattering states of $\eta_b K^*$, $\Upsilon K^{(*)}$ and $B^{(*)} B_s^{(*)}$ are clearly identified in the energy region 9.0–11.3 GeV. Since there are dense distributions of radial excited states, two energy intervals, 10.65–10.80 GeV and 11.05–11.20 GeV, are plotted in the middle and bottom panels, respectively. Apart from three scattering states of $B^*(1S)B_s(1S)$, $B(1S)B_s^*(1S)$ and $B^*(1S)B_s^*(1S)$ obtained in the middle panel, no resonance is available. Three narrow resonance poles are found in the bottom panel. Their complex energies are $11178 + i0.8$ GeV, $11086 + i1.0$ GeV and $11092 + i1.1$ GeV. By considering the location of the resonance poles, the $\eta_b(1S)K^*(2S)$ should be the dominant decay channel of the two lower-energy resonances, whereas the

$\Upsilon(1S)K^*(2S)$ channel must play a dominant role for the remaining resonance.

The $I(J^P) = \frac{1}{2}(2^+)$ sector: From Table XII, we can see that the 14 contributing channels are all above 10.41 GeV and the lowest mass is 10412 MeV, which is just the theoretical value of ΥK^* threshold. Moreover, this fact remains unchanged when a complete coupled-channel calculation is performed in real-range formulation.

In a complex-range investigation in which the rotated angle is varied from 0° to 6° , the scattering states of ΥK^* and $B^* B_s^*$ are well identified in Fig. 10. Particularly, they are located within an energy interval 10.4–11.6 GeV. It is worth noting that a stable resonance is obtained above the threshold lines of $\Upsilon(2S)K^*(1S)$, and the calculated pole is $11090 + i1.1$ MeV.

TABLE XII. Lowest-lying $b\bar{b}u\bar{s}$ tetraquark states with $I(J^P) = \frac{1}{2}(2^+)$ calculated within the real range formulation of the chiral quark model. The results are similarly organized as those in Table IV. (unit: MeV).

Channel	Index	$\chi_i^{\sigma_i}; \chi_I^{f_j}; \chi_k^c$ [$i; j; k$]	M	Mixed
$(\Upsilon K^*)^1(10352)$	1	[1; 2; 1]	10412	
$(B^* \bar{B}_s^*)^1(10740)$	2	[1; 2; 1]	10719	10412
$(\Upsilon K^*)^8$	3	[1; 2; 2]	11000	
$(B^* \bar{B}_s^*)^8$	4	[1; 2; 2]	10843	10785
$(bu)^*(\bar{s}\bar{b})^*$	5	[1; 2; 3]	10890	
$(bu)^*(\bar{s}\bar{b})^*$	6	[1; 2; 4]	10839	10707
K_1	7	[1; 2; 5]	10994	
	8	[1; 2; 6]	10701	10701
K_2	9	[1; 2; 7]	10696	
	10	[1; 2; 6]	10994	10696
K_3	11	[1; 2; 9]	10830	
	12	[1; 2; 10]	10881	10707
K_4	13	[1; 2; 11]	10838	
	14	[1; 2; 12]	10883	10705
Complete coupled-channels:			10412	

TABLE XIII. Lowest-lying $b\bar{b}s\bar{s}$ tetraquark states with $I(J^P) = 0(0^+)$ calculated within the real range formulation of the chiral quark model. The results are similarly organized as those in Table IV. (unit: MeV).

Channel	Index	$\chi_i^{\sigma_i}; \chi_I^{f_j}; \chi_k^c$ [$i; j; k$]	M	Mixed
$(\eta_b \eta')^1(9848)$	1	[1; 3; 1]	10282	
$(\Upsilon \phi)^1(10242)$	2	[2; 3; 1]	10516	
$(B_s \bar{B}_s)^1(10560)$	3	[1; 3; 1]	10710	
$(B_s^* \bar{B}_s^*)^1(10650)$	4	[2; 3; 1]	10800	10282
$(\eta_b \eta')^8$	5	[1; 3; 2]	11102	
$(\Upsilon \phi)^8$	6	[2; 3; 2]	11068	
$(B_s \bar{B}_s)^8$	7	[1; 3; 2]	10983	
$(B_s^* \bar{B}_s^*)^8$	8	[2; 3; 2]	10938	10822
$(bs)(\bar{s}\bar{b})$	9	[3; 3; 3]	10972	
$(bs)(\bar{s}\bar{b})$	10	[3; 3; 4]	10967	
$(bs)^*(\bar{s}\bar{b})^*$	11	[4; 3; 3]	10952	
$(bs)^*(\bar{s}\bar{b})^*$	12	[4; 3; 4]	10886	10745
K_1	13	[5; 3; 5]	11064	
	14	[6; 3; 5]	11097	
	15	[5; 3; 6]	10815	
	16	[6; 3; 6]	10712	10711
K_3	17	[9; 3; 9]	10880	
	18	[10; 3; 9]	10951	
	19	[9; 3; 10]	10958	
	20	[10; 3; 10]	10967	10740
Complete coupled-channels:			10282	

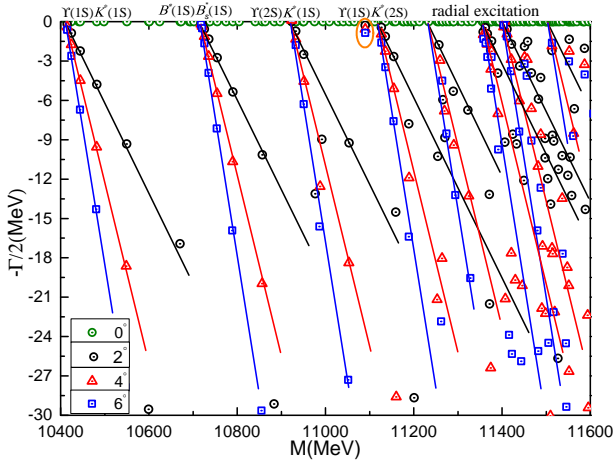


FIG. 10. The complete coupled-channels calculation of the $b\bar{b}u\bar{s}$ tetraquark system with $I(J^P) = \frac{1}{2}(2^+)$ quantum numbers. We use the complex-scaling method of the chiral quark model varying θ from 0° to 6° .

C. The $b\bar{b}s\bar{s}$ tetraquarks

The last sector of hidden-bottom tetraquarks in our investigation is the $b\bar{b}s\bar{s}$ system. Three spin-parity states, $J^P = 0^+, 1^+$ and 2^+ , with isospin $I = 0$, are studied. As

in the $b\bar{b}q\bar{q}$ ($q = u, d$) system, due to symmetry properties of the Hamiltonian with respect to the K-type configurations, only K_1 and K_3 arrangements are sufficient to consider. In summary, only one extremely narrow resonance is obtained in the $I(J^P) = 0(1^+)$ channel.

The $I(J^P) = 0(0^+)$ sector: Table XIII lists the calculated masses of the $0(0^+)$ $b\bar{b}s\bar{s}$ tetraquark system. Firstly, no bound state is found in each single channel, and also in the different variants of the coupled-channels calculations. The lowest mass obtained is 10282 MeV, which is just the theoretical value of $\eta_b \eta'$ threshold. The remaining channels are generally located within an energy interval 10.5 – 11.1 GeV.

When a fully coupled-channel calculation is performed using the complex-range method, the scattering nature of $\eta_b \eta'$, $\Upsilon \phi$ and $B_s^{(*)} \bar{B}_s^{(*)}$ are clearly shown in Fig. 11. Generally, no stable pole is found in the top panel. Besides, an enlarged energy region from 11.35 GeV to 11.50 GeV is presented in the bottom panel, the radial excitations $\Upsilon(3S)\phi(1S)$, $B_s(1S)\bar{B}_s(2S)$ and $B_s^*(1S)\bar{B}_s^*(2S)$ are shown no resonance is obtained, too.

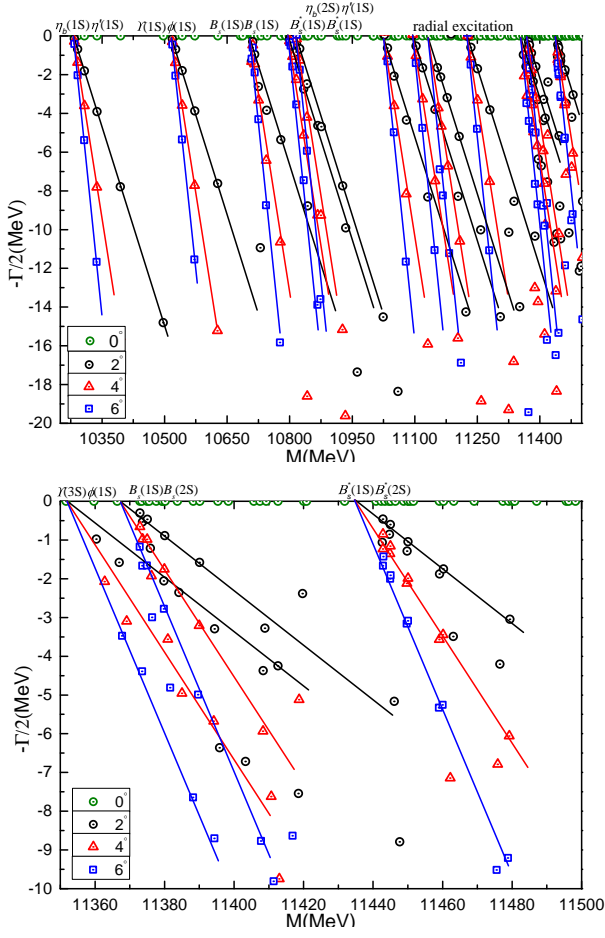


FIG. 11. *Top panel:* The complete coupled-channels calculation of the $b\bar{b}s\bar{s}$ tetraquark system with $I(J^P) = 0(0^+)$ quantum numbers. *Bottom panel:* Enlarged top panel, with real values of energy ranging from 11.35 GeV to 11.50 GeV. We use the complex-scaling method of the chiral quark model varying θ from 0° to 6° .

The $I(J^P) = 0(1^+)$ sector: 26 channels contribute to the $b\bar{b}s\bar{s}$ tetraquark system with $0(1^+)$ quantum numbers. The five color-singlet meson-meson channels, $\eta_b\phi$, $\Upsilon\eta'$, $\Upsilon\phi$ and $B_s^{(*)}\bar{B}_s^{(*)}$, are all scattering states and the lowest mass 10333 GeV is just the value of non-interacting $\Upsilon\eta'$ threshold. The other exotic quark arrangements are generally located in 10.76 – 11.10 GeV. Meanwhile, coupled-channel has little effect on these results.

Figure 12 presents distributions of $\eta_b\phi$, $\Upsilon\eta'$, $\Upsilon\phi$ and $B_s^{(*)}\bar{B}_s^{(*)}$ channels, in both ground and radial excitation states, when coupled-channel calculation is performed with CSM employed. One extremely narrow resonance is found circled above $\Upsilon(1S)\phi(2S)$ threshold. The calculated complex-energy is $11280 + i0.4$ MeV. The quite narrow resonance width indicates that it should be stable against two-mesons strong decay processes.

The $I(J^P) = 0(2^+)$ sector: Table XV shows all the channels that can contribute to the mass of the

TABLE XIV. Lowest-lying $b\bar{b}s\bar{s}$ tetraquark states with $I(J^P) = 0(1^+)$ calculated within the real range formulation of the chiral quark model. The results are similarly organized as those in Table IV. (unit: MeV).

Channel	Index	$\chi_J^{\sigma_i}; \chi_I^{f_j}; \chi_k^c$ [$i; j; k$]	M	Mixed
$(\eta_b\phi)^1(10082)$	1	[1; 3; 1]	10465	
$(\Upsilon\eta')^1(10008)$	2	[2; 3; 1]	10333	
$(\Upsilon\phi)^1(10242)$	3	[3; 3; 1]	10516	
$(B_s\bar{B}_s^*)^1(10605)$	4	[1; 3; 1]	10755	
$(B_s^*\bar{B}_s)^1(10650)$	5	[3; 3; 1]	10800	10333
$(\eta_b\phi)^8$	6	[1; 3; 2]	11082	
$(\Upsilon\eta')^8$	7	[2; 3; 2]	11102	
$(\Upsilon\phi)^8$	8	[3; 3; 2]	11075	
$(B_s\bar{B}_s^*)^8$	9	[1; 3; 2]	10985	
$(B_s^*\bar{B}_s)^8$	10	[3; 3; 2]	10951	10848
$(bs)(\bar{s}\bar{b})^*$	11	[4; 3; 3]	10986	
$(bs)(\bar{s}\bar{b})^*$	12	[4; 3; 4]	10969	
$(bs)^*(\bar{s}\bar{b})^*$	13	[6; 3; 3]	10949	
$(bs)^*(\bar{s}\bar{b})^*$	14	[6; 3; 4]	10902	10782
K_1	15	[7; 3; 5]	11090	
	16	[8; 3; 5]	11081	
	17	[9; 3; 5]	11080	
	18	[7; 3; 6]	10782	
	19	[8; 3; 6]	10799	
	20	[9; 3; 6]	10764	10763
K_3	21	[13; 3; 9]	10905	
	22	[14; 3; 9]	10910	
	23	[15; 3; 9]	10946	
	24	[13; 3; 10]	10954	
	25	[14; 3; 10]	10953	
	26	[15; 3; 10]	10979	10770
Complete coupled-channels:			10333	

highest spin state of $b\bar{b}s\bar{s}$ tetraquark. No bound state is still found in the single- and coupled-channel calculations, with the lowest mass indicating the value of $\Upsilon\phi$ threshold, 10516 MeV. Our results of a complete coupled-channel calculation in complex-range are shown in Fig. 13. Therein, one can find that $\Upsilon\phi$ and $B_s^*\bar{B}_s^*$ scattering states are well presented in 10.5 – 11.5 GeV, and no stable resonance pole is acquired.

IV. SUMMARY

The bottomonium-like tetraquarks $b\bar{b}q\bar{q}$ ($q = u, d, s$) with spin-parity $J^P = 0^+, 1^+$ and 2^+ , and isospin

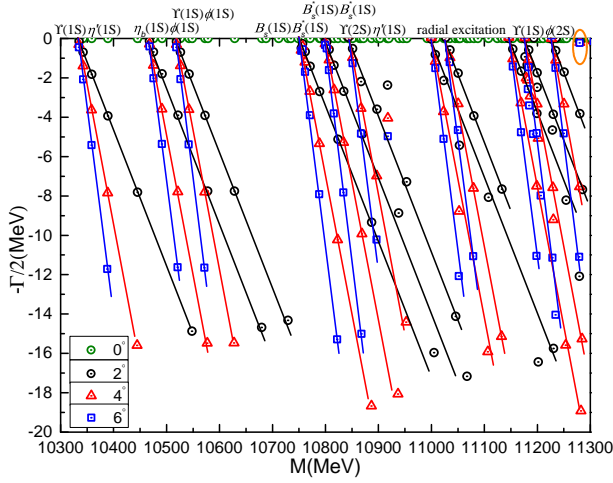


FIG. 12. The complete coupled-channels calculation of the $b\bar{b}s\bar{s}$ tetraquark system with $I(J^P) = 0(1^+)$ quantum numbers. We use the complex-scaling method of the chiral quark model varying θ from 0° to 6° .

TABLE XV. Lowest-lying $b\bar{b}s\bar{s}$ tetraquark states with $I(J^P) = 0(2^+)$ calculated within the real range formulation of the chiral quark model. The results are similarly organized as those in Table IV. (unit: MeV).

Channel	Index	$\chi_J^{\sigma i}; \chi_I^{f j}; \chi_k^c$ [$i; j; k$]	M	Mixed
$(\Upsilon\phi)^1(10242)$	1	[1; 3; 1]	10516	
$(B_s^*\bar{B}_s^*)^1(10650)$	2	[1; 3; 1]	10800	10516
$(\Upsilon\phi)^8$	3	[1; 3; 2]	11090	
$(B_s^*\bar{B}_s^*)^8$	4	[1; 3; 2]	10974	10886
$(bs)^*(\bar{s}\bar{b})^*$	5	[1; 3; 3]	10972	
$(bs)^*(\bar{s}\bar{b})^*$	6	[1; 3; 4]	10931	10822
K_1	7	[1; 3; 5]	11088	
	8	[1; 3; 6]	10815	10815
K_3	9	[1; 3; 9]	10928	
	10	[1; 3; 10]	10962	10823
Complete coupled-channels:				10516

$I = 0, 1$ or $\frac{1}{2}$, are systematically investigated by means of real- and complex-scaling range formulation of a chiral quark model, along with a high efficiency numerical approach for solving the 4-body Schrödinger equation, the Gaussian expansion method. The model contains one-gluon exchange, linear-screened color confining and Goldstone-boson exchanges (between light quarks) interactions, and it has been successfully applied to the description of hadron, hadron-hadron and multiquark phenomenology. We considered in our calculations all possi-

ble tetraquark arrangements allowed by quantum num-

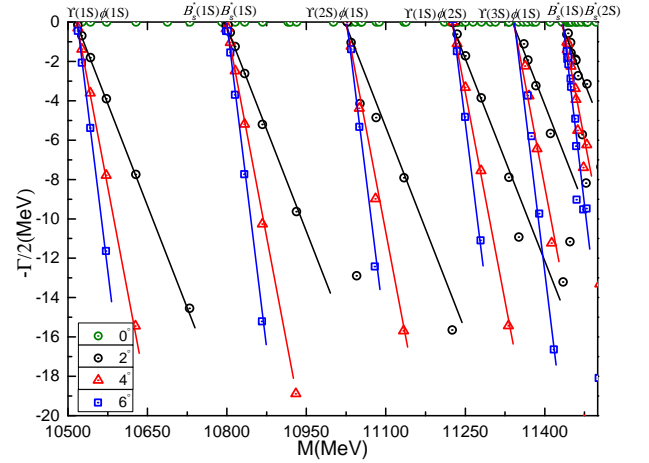


FIG. 13. The complete coupled-channels calculation of the $b\bar{b}s\bar{s}$ tetraquark system with $I(J^P) = 0(2^+)$ quantum numbers. We use the complex-scaling method of the chiral quark model varying θ from 0° to 6° .

bers: singlet- and hidden-color meson-meson configurations, diquark-antidiquark arrangements with their allowed color triplet-antitriplet and sextet-antisextet wave functions, and four K-type structures.

Several resonance structures are found in a complete coupled-channel calculation. They are summarized in Table XVI which collects quantum numbers, dominant channel and pole position in the complex energy-plane. A brief review of them is as follows. On one hand, in the $b\bar{b}q\bar{q}$ ($q = u, d$) tetraquark system, we found resonance states of $B^{(*)}\bar{B}^{(*)}$, $\Upsilon\omega$, $\Upsilon\rho$ and $\eta_b\rho$ nature with all possible $I(J^P)$ quantum numbers. Their masses are generally located in the energy range 11.0–11.3 GeV and their widths are less than 10 MeV. On the other hand, extremely narrow resonances, with two-meson strong decay widths less than 1.5 MeV, are obtained in both $b\bar{b}u\bar{s}$ and $b\bar{b}s\bar{s}$ tetraquark systems. Particularly, four radial excitations of ΥK^* and $\eta_b K^*$ are found at ~ 11.1 GeV in $J^P = 0^+, 1^+$ and 2^+ channels of $b\bar{b}u\bar{s}$ system. One $\Upsilon(1S)\phi(2S)$ resonance state is obtained at 11.28 GeV in the $J^P = 1^+$ sector.

ACKNOWLEDGMENTS

Work partially financed by: the Zhejiang Provincial Natural Science Foundation under Grant No. LQ22A050004; National Natural Science Foundation of China under Grant Nos. 11535005 and 11775118; the Ministerio Español de Ciencia e Innovación under grant No. PID2019-107844GB-C22; and Junta de Andalucía, contract nos. P18-FR-5057 and Operativo FEDER Andalucía 2014-2020 UHU-1264517.

TABLE XVI. Summary of resonance structures found in the $b\bar{b}q\bar{q}$ ($q = u, d, s$) tetraquark systems. The first column shows the isospin, total spin and parity quantum numbers of each singularity, the second column refers to the dominant channel, the obtained resonances are presented with the following notation: $E = M + i\Gamma$ in the last column. (unit: MeV).

$I(J^P)$	Dominant Channel	Complex Energy
$b\bar{b}q\bar{q}$ ($q = u, d$) tetraquarks		
$0(0^+)$	$B(1S)\bar{B}(2S)$	$11322 + i3.9$
	$B(1S)\bar{B}(2S)$	$11328 + i3.4$
$0(1^+)$	$B(1S)\bar{B}^*(1S)$	$10584 + i1.6$
	$\Upsilon(3S)\omega(1S)$	$11073 + i1.8$
	$\Upsilon(3S)\omega(1S)$	$11209 + i2.8$
	$\Upsilon(3S)\omega(1S)$	$11272 + i5.0$
$0(2^+)$	$B^*(1S)\bar{B}^*(1S)$	$10618 + i1.0$
	$B(1S)\bar{B}^*(2S)$	$11416 + i32.6$
$1(0^+)$	$\Upsilon(2S)\rho(1S)$	$10935 + i1.4$
$1(1^+)$	$B^*(1S)\bar{B}^*(1S)$	$10750 + i1.0$
	$\eta_b(1S)\rho(2S)$	$10960 + i0.7$
	$\eta_b(1S)\rho(2S)$	$10967 + i2.6$
$1(2^+)$	$B^*(1S)\bar{B}^*(2S)$	$11390 + i7.8$
$b\bar{b}u\bar{s}$ tetraquarks		
$\frac{1}{2}(0^+)$	$\Upsilon(1S)K^*(2S)$	$11176 + i0.8$
$\frac{1}{2}(1^+)$	$\eta_b(1S)K^*(2S)$	$11178 + i0.8$
	$\eta_b(1S)K^*(2S)$	$11086 + i1.0$
	$\Upsilon(1S)K^*(2S)$	$11092 + i1.1$
$\frac{1}{2}(2^+)$	$\Upsilon(2S)K^*(1S)$	$11090 + i1.1$
$b\bar{b}s\bar{s}$ tetraquarks		
$0(1^+)$	$\Upsilon(1S)\phi(2S)$	$11280 + i0.4$

- [1] R. Aaij *et al.* (LHCb), *Phys. Rev. Lett.* **115**, 072001 (2015).
- [2] R. Aaij *et al.* (LHCb), *Phys. Rev. Lett.* **122**, 222001 (2019).
- [3] R. Aaij *et al.* (LHCb), *Phys. Rev. Lett.* **128**, 062001 (2022), arXiv:2108.04720 [hep-ex].
- [4] R. Aaij *et al.* (LHCb), *Sci. Bull.* **66**, 1391 (2021), arXiv:2012.10380 [hep-ex].
- [5] R. Aaij *et al.* (LHCb), *Phys. Rev. D* **102**, 112003 (2020), arXiv:2009.00026 [hep-ex].
- [6] R. Aaij *et al.* (LHCb), *Phys. Rev. Lett.* **125**, 242001 (2020), arXiv:2009.00025 [hep-ex].
- [7] R. Aaij *et al.* (LHCb), (2021), arXiv:2109.01038 [hep-ex].
- [8] R. Aaij *et al.* (LHCb), (2021), arXiv:2109.01056 [hep-ex].
- [9] M. Ablikim *et al.* (BESIII), *Phys. Rev. Lett.* **126**, 102001 (2021), arXiv:2011.07855 [hep-ex].
- [10] R. Aaij *et al.* (LHCb), *Phys. Rev. Lett.* **127**, 082001 (2021), arXiv:2103.01803 [hep-ex].
- [11] R. Aaij *et al.* (LHCb), *Sci. Bull.* **65**, 1983 (2020), arXiv:2006.16957 [hep-ex].
- [12] A. Bondar *et al.* (Belle), *Phys. Rev. Lett.* **108**, 122001 (2012), arXiv:1110.2251 [hep-ex].
- [13] A. Garmash *et al.* (Belle), *Phys. Rev. D* **91**, 072003 (2015), arXiv:1403.0992 [hep-ex].
- [14] A. Garmash *et al.* (Belle), *Phys. Rev. Lett.* **116**, 212001 (2016), arXiv:1512.07419 [hep-ex].
- [15] M. Cleven, F.-K. Guo, C. Hanhart, and U.-G. Meissner, *Eur. Phys. J. A* **47**, 120 (2011), arXiv:1107.0254 [hep-ph].
- [16] J. He, *Phys. Rev. D* **90**, 076008 (2014), arXiv:1409.8506 [hep-ph].
- [17] Z.-F. Sun, J. He, X. Liu, Z.-G. Luo, and S.-L. Zhu, *Phys. Rev. D* **84**, 054002 (2011), arXiv:1106.2968 [hep-ph].
- [18] Y.-C. Yang, Z.-Y. Tan, H.-S. Zong, and J. Ping, *Few Body Syst.* **60**, 9 (2019), arXiv:1712.09285 [hep-ph].

- [19] L. Zhang, X.-W. Kang, and X.-H. Guo, (2022), arXiv:2203.02301 [hep-ph].
- [20] J. Nieves and M. P. Valderrama, *Phys. Rev. D* **84**, 056015 (2011), arXiv:1106.0600 [hep-ph].
- [21] J. M. Dias, F. Aceti, and E. Oset, *Phys. Rev. D* **91**, 076001 (2015), arXiv:1410.1785 [hep-ph].
- [22] F. K. Guo, C. Hanhart, Y. S. Kalashnikova, P. Matuschek, R. V. Mizuk, A. V. Nefediev, Q. Wang, and J. L. Wynen, *Phys. Rev. D* **93**, 074031 (2016), arXiv:1602.00940 [hep-ph].
- [23] Q. Wang, V. Baru, A. A. Filin, C. Hanhart, A. V. Nefediev, and J. L. Wynen, *Phys. Rev. D* **98**, 074023 (2018), arXiv:1805.07453 [hep-ph].
- [24] P. G. Ortega, J. Segovia, and F. Fernandez, *Phys. Rev. D* **104**, 094004 (2021), arXiv:2107.02544 [hep-ph].
- [25] M. Sadi and S. Prelovsek, *Phys. Rev. D* **104**, 114503 (2021), arXiv:2109.08560 [hep-lat].
- [26] L. R. Dai, E. Oset, A. Feijoo, R. Molina, L. Roca, A. M. Torres, and K. P. Khemchandani, (2022), arXiv:2201.04840 [hep-ph].
- [27] F. Goerke, T. Gutsche, M. A. Ivanov, J. G. Körner, and V. E. Lyubovitskij, *Phys. Rev. D* **96**, 054028 (2017), arXiv:1707.00539 [hep-ph].
- [28] G.-J. Wang, X.-H. Liu, L. Ma, X. Liu, X.-L. Chen, W.-Z. Deng, and S.-L. Zhu, *Eur. Phys. J. C* **79**, 567 (2019), arXiv:1811.10339 [hep-ph].
- [29] X.-K. Dong, F.-K. Guo, and B.-S. Zou, *Phys. Rev. Lett.* **126**, 152001 (2021), arXiv:2011.14517 [hep-ph].
- [30] H.-X. Chen, W. Chen, X. Liu, and S.-L. Zhu, *Phys. Rept.* **639**, 1 (2016), arXiv:1601.02092 [hep-ph].
- [31] H.-X. Chen, W. Chen, X. Liu, Y.-R. Liu, and S.-L. Zhu, *Rept. Prog. Phys.* **80**, 076201 (2017), arXiv:1609.08928 [hep-ph].
- [32] F.-K. Guo, C. Hanhart, U.-G. Meißner, Q. Wang, Q. Zhao, and B.-S. Zou, *Rev. Mod. Phys.* **90**, 015004 (2018), arXiv:1705.00141 [hep-ph].
- [33] Y.-R. Liu, H.-X. Chen, W. Chen, X. Liu, and S.-L. Zhu, *Prog. Part. Nucl. Phys.* **107**, 237 (2019), arXiv:1903.11976 [hep-ph].
- [34] G. Yang, J. Ping, and J. Segovia, *Symmetry* **12**, 1869 (2020), arXiv:2009.00238 [hep-ph].
- [35] X.-K. Dong, F.-K. Guo, and B.-S. Zou, *Commun. Theor. Phys.* **73**, 125201 (2021), arXiv:2108.02673 [hep-ph].
- [36] H.-X. Chen, (2021), arXiv:2103.08586 [hep-ph].
- [37] G. Yang, J. Ping, and J. Segovia, *Phys. Rev. D* **104**, 094035 (2021), arXiv:2109.04311 [hep-ph].
- [38] G. Yang, J. Ping, and F. Wang, *Phys. Rev. D* **95**, 014010 (2017).
- [39] G. Yang, J. L. Ping, and J. Segovia, *Phys. Rev. D* **101**, 074030 (2020).
- [40] G. Yang, J. Ping, and J. Segovia, *Phys. Rev. D* **99**, 014035 (2019).
- [41] G. Yang, J. L. Ping, and J. Segovia, *Phys. Rev. D* **101**, 014001 (2020).
- [42] G. Yang, J. Ping, and J. Segovia, *Phys. Rev. D* **102**, 054023 (2020).
- [43] G. Yang, J. Ping, and J. Segovia, *Phys. Rev. D* **104**, 014006 (2021), arXiv:2104.08814 [hep-ph].
- [44] G. Yang, J. Ping, and J. Segovia, *Phys. Rev. D* **103**, 074011 (2021), arXiv:2101.04933 [hep-ph].
- [45] J. Aguilar and J. M. Combes, *Commun. Math. Phys.* **22**, 269 (1971).
- [46] E. Balslev and J. M. Combes, *Commun. Math. Phys.* **22**, 280 (1971).
- [47] J. Vijande, F. Fernandez, and A. Valcarce, *J. Phys. G* **31**, 481 (2005), arXiv:hep-ph/0411299 [hep-ph].
- [48] M. D. Scadron, *Phys. Rev. D* **26**, 239 (1982).
- [49] R. Garcia-Martin, R. Kaminski, J. R. Pelaez, and J. Ruiz de Elvira, *Phys. Rev. Lett.* **107**, 072001 (2011), arXiv:1107.1635 [hep-ph].
- [50] M. Albaladejo and J. A. Oller, *Phys. Rev. D* **86**, 034003 (2012), arXiv:1205.6606 [hep-ph].
- [51] J. R. Pelaez, *Phys. Rept.* **658**, 1 (2016), arXiv:1510.00653 [hep-ph].
- [52] G. S. Bali, H. Neff, T. Duessel, T. Lippert, and K. Schilling (SESAM), *Phys. Rev. D* **71**, 114513 (2005), arXiv:hep-lat/0505012 [hep-lat].
- [53] J. Segovia, D. R. Entem, and F. Fernandez, *Phys. Lett. B* **662**, 33 (2008).
- [54] J. Segovia, D. R. Entem, F. Fernandez, and E. Hernandez, *Int. J. Mod. Phys. E* **22**, 1330026 (2013), arXiv:1309.6926 [hep-ph].
- [55] J. Segovia, A. Yasser, D. Entem, and F. Fernandez, *Phys. Rev. D* **80**, 054017 (2009).
- [56] J. Segovia, D. Entem, and F. Fernandez, *Phys. Rev. D* **83**, 114018 (2011).
- [57] J. Segovia, D. R. Entem, and F. Fernandez, *Phys. Rev. D* **91**, 094020 (2015), arXiv:1502.03827 [hep-ph].
- [58] J. Segovia, P. G. Ortega, D. R. Entem, and F. Fernández, *Phys. Rev. D* **93**, 074027 (2016), arXiv:1601.05093 [hep-ph].
- [59] G. Yang, J. Ping, and J. Segovia, *Few-Body Syst.* **59**, 113 (2018), arXiv:1709.09315 [hep-ph].
- [60] G. Yang, J. Ping, P. G. Ortega, and J. Segovia, *Chin. Phys. C* **44**, 023102 (2020), arXiv:1904.10166 [hep-ph].
- [61] P. G. Ortega, J. Segovia, D. R. Entem, and F. Fernandez, *Phys. Rev. D* **94**, 074037 (2016), arXiv:1603.07000 [hep-ph].
- [62] P. G. Ortega, J. Segovia, D. R. Entem, and F. Fernández, *Phys. Rev. D* **95**, 034010 (2017), arXiv:1612.04826 [hep-ph].
- [63] P. G. Ortega, J. Segovia, D. R. Entem, and F. Fernández, *Phys. Rev. D* **94**, 114018 (2016), arXiv:1608.01325 [hep-ph].
- [64] P. G. Ortega, J. Segovia, D. R. Entem, and F. Fernández, *Phys. Lett. B* **778**, 1 (2018), arXiv:1706.02639 [hep-ph].
- [65] P. G. Ortega, J. Segovia, D. R. Entem, and F. Fernández, *Eur. Phys. J. C* **79**, 78 (2019), arXiv:1808.00914 [hep-ph].
- [66] P. G. Ortega, J. Segovia, D. R. Entem, and F. Fernandez, *Eur. Phys. J. C* **80**, 223 (2020), arXiv:2001.08093 [hep-ph].
- [67] G. Yang and J. Ping, *Phys. Rev. D* **97**, 034023 (2018), arXiv:1703.08845 [hep-ph].
- [68] G. Yang, J. Ping, and J. Segovia, *Phys. Rev. D* **102**, 054023 (2020), arXiv:2007.05190 [hep-ph].
- [69] G. Yang, J. Ping, and J. Segovia, *Phys. Rev. D* **101**, 074030 (2020), arXiv:2003.05253 [hep-ph].
- [70] E. Hiyama, Y. Kino, and M. Kamimura, *Prog. Part. Nucl. Phys.* **51**, 223 (2003).